Titanium Imido Complexes of Cyclooctatetraenyl Ligands

Simon C. Dunn,[a] Nilay Hazari,[a] Nicholas M. Jones,[a] Aidan G. Moody,[a] Alexander J. Blake,[b] Andrew R. Cowley,[a] Jennifer C. Green,[a] and Philip Mountford*[a]

Abstract: Reaction of $[Ti(NR)Cl_2(py)_3]$ (R = *t*Bu or 2,6-*i*$Pr_2C_6H_3$) with $K_2[COT]$ (COT = C_8H_8) or $Li_2[COT'']$ (COT'' = 1,4-$C_8H_6(SiMe_3)_2$) gave the monomeric complexes $[Ti(NR)(\eta^8\text{-}COT)]$ or $[Ti(NR)(\eta^8\text{-}COT'')]$, respectively. The pseudo-two coordinate, 'pogo stick' geometry for these complexes is unique in both early transition-metal and cyclooctatetraenyl ligand chemistry. In contrast, reaction of $[Ti(N\text{-}2,6\text{-}Me_2C_6H_3)Cl_2(py)_3]$ with $K_2[COT]$ gave the μ-imido-bridged dimer $[Ti_2(\mu\text{-}N\text{-}2,6\text{-}Me_2C_6H_3)_2(\eta^8\text{-}COT)_2]$. It appears that as the steric bulk of the imido and C_8 ring substituents are decreased, dimerisation becomes more favourable. Aryl imido COT complexes were also prepared by imido ligand exchange reactions between anilines and $[Ti(NtBu)(\eta^8\text{-}COT)]$ or $[Ti(NtBu)(\eta^8\text{-}COT'')]$. The complexes $[Ti(NtBu)(\eta^8\text{-}COT)]$, $[Ti(N\text{-}2,6\text{-}iPr_2C_6H_3)_2(\eta^8\text{-}COT)]$ and $[Ti_2(\mu\text{-}N\text{-}2,6\text{-}Me_2C_6H_3)_2(\eta^8\text{-}COT)_2]$ have been crystallographically characterised. The electronic structures of both the monomeric and dimeric complexes have been investigated by using density functional theory (DFT) calculations and gas-phase photoelectron spectroscopy. The most striking aspect of the bonding is that binding to the imido nitrogen atom is primarily through σ and π interactions, whereas that to the COT or COT'' ring is almost exclusively through δ symmetry orbitals. A DFT-based comparison between the bonding in $[Ti(NtBu)(\eta^8\text{-}COT)]$ and the bonding in the previously reported late transition-metal 'pogo-stick' complexes $[Os(NtBu)(\eta^6\text{-}C_6Me_6)]$, $[Ir(NtBu)(\eta^5\text{-}C_5Me_5)]$ and $[Ni(NO)(\eta^5\text{-}C_5H_5)]$ has also been undertaken.

Keywords: cyclooctatetraenyl ligands · density functional calculations · imido compounds · photoelectron spectroscopy · titanium

Introduction

Over the last 15 years, the chemistry of Group 4 transition-metal imides has received considerable attention.[1–7] Both computational and experimental studies have been performed to probe the structure and reactivity of these systems. It has been shown that Group 4 transition-metal imides have potential in C–H activation chemistry,[8–16] materials chemistry[17–20] and olefin polymerisation catalysis (with the imide acting as an "ancillary ligand"),[21–23] and that these systems can be utilised in an wide variety of stoichiometric and sometimes catalytic coupling reactions with unsaturated substrates.[6] Terminal titanium imido complexes were first structurally characterised in 1990,[24,25] and since then a large number of imido complexes with different ancillary ligands have been synthesised.[6] A general entry point to new titanium imido chemistry is gained by way of the readily prepared synthons $[Ti(NR)Cl_2(py)_3]$ (R = *t*Bu or aryl) and their homologues, from which straightforward metathesis reactions afford a wide range of derivatives.[26]

We noticed that although cyclopentadienyl and to a lesser extent arene co-ligands have been widely used in transition-metal imido chemistry, there has only been one report of imido complexes bearing cyclooctatetraenyl co-ligands, namely the dinuclear μ-arylimido derivatives $[M_2(\mu\text{-}N\text{-}2,6\text{-}iPr_2C_6H_3)_2(\eta^8\text{-}COT)_2]$ (M = Zr, Hf).[27] Therefore, we were interested to see if using the smaller titanium congener would lead to a mononuclear derivative. Only two families of one-legged piano stool ('pogo stick') imido complexes

[a] Dr. S. C. Dunn, N. Hazari, N. M. Jones, Dr. A. G. Moody, Dr. A. R. Cowley, Prof. J. C. Green, Dr. P. Mountford
Inorganic Chemistry Laboratory, University of Oxford
South Parks Road, Oxford OX1 3QR (UK)
Fax: (+44) 1865-285-141
E-mail: philip.mountford@chem.ox.ac.uk

[b] Dr. A. J. Blake
Department of Chemistry, University of Nottingham
Nottingham NG7 2RD (UK)

Supporting information for this article is available on the WWW under http://www.chemeurj.org/ or from the author. X-ray crystallographic files in CIF format for the structure determination of compounds **1**, **3** and **6**; optimised geometries in cartesian (*xyz*) form for compounds **1**, **2**, **3**, **6**, **9**, **12**, **13**, **14**, **15** and **16**; details of fragment analyses for compounds **14**, **15** and **16**; and comparison of selected experimental and calculated bond lengths for **15** and **16**.

 DOI: 10.1002/chem.200401104

have been reported previously and both consisted of later transition-metal, 18-valence-electron compounds of the type $[Ir(\eta^5\text{-}C_5Me_5)(NR)]$[28] (R = *t*Bu, $SiMe_2$*t*Bu, 2,6-$Me_2C_6H_6$ or 2,6-*i*$Pr_2C_6H_6$) and $[Os(\eta^6\text{-}C_6Me_6)(N$*t*$Bu)]$ or $[Os(\eta^6$-*p*-cymene$)(NR)]$ (R = *t*Bu or 2,6-$Me_2C_6H_6$).[29] Here we report a unique series of monomeric and dimeric cyclooctatetraenyl titanium imido complexes whose structures depend on the steric bulk of the imido and/or C_8 ring substituents. We describe the solid-state structures of two of the novel pseudo-two-coordinate titanium imido species, along with a computational study of the electronic structure of cyclooctatetraenyl titanium imido complexes. Part of this work has been communicated previously.[30]

Results and Discussion

Synthesis and characterisation of cyclooctatetraenyl titanium imido complexes: Titanium imido dichloride starting materials $[Ti(NR)Cl_2(py)_3]$ (R = *t*Bu, 2,6-$Me_2C_6H_3$, 2,6-*i*$Pr_2C_6H_3$ and 2-*t*BuC_6H_4) were prepared according to previously described routes.[21,26] Reaction of these with either $K_2[COT]$ (COT = C_8H_8) or the more sterically bulky $Li_2[COT'']\cdot 1.8\,THF$ (COT″ = 1,4-bis(trimethylsilyl)-1,3,5,7-cyclooctatetraenyl) gave products that depended critically on the exact nature of both the imido and cyclooctatetraenyl ring substituents. Addition of one equivalent of either $K_2[COT]$ or $Li_2[COT'']\cdot 1.8\,THF$ to $[Ti(N$*t*$Bu)Cl_2(py)_3]$ in THF at −50 °C gave a dark red solution. After standard work-up, spectroscopically clean samples of the pseudo-two-coordinate complexes $[Ti(N$*t*$Bu)(COT)]$ (**1**) or $[Ti(N$*t*$Bu)(COT'')]$ (**2**), respectively, were isolated as yellow solids [Eq. (1)]. The NMR spectra of **1** contained singlet resonances for a *tert*-butylimido group and an η^8-coordinated COT ring. The ^{1}H NMR spectrum of **2** was more complicated due to the decrease in symmetry in the COT″ ring. In this case the precise assignments of the COT″ protons were determined by using NOE difference spectroscopy. The nuclearity of **1** was confirmed by X-ray diffraction analysis (vide infra), and by analogy **2** is also proposed to be monomeric. The presence of the $SiMe_3$ groups on the COT ring appears to increase the solubility of **2** in hydrocarbon solvents relative to **1**.

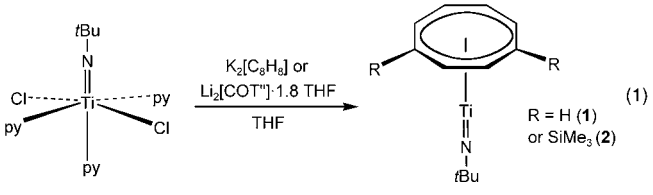

(1)

The methodology used to synthesise **1** and **2** was extended to prepare titanium COT complexes which contain aryl imido substituents. The reactions of the aryl imido precursors $[Ti(NR)Cl_2(py)_3]$ (R = 2,6-$Me_2C_6H_3$, 2,6-*i*$Pr_2C_6H_3$ and 2-*t*BuC_6H_4) with either $K_2[COT]$ or $Li_2[COT'']\cdot 1.8\,THF$ gave two types of products depending on the exact nature of the cyclooctatetraenyl ligand. The reaction of [Ti(N-2,6-*i*$Pr_2C_6H_3$)$Cl_2(py)_3$] with $K_2[COT]$ in THF gave the crystallographically characterised (vide infra) monomeric orange complex [Ti(N-2,6-*i*$Pr_2C_6H_3$)(COT)] (**3**). Although [Ti(N-2,6-*i*$Pr_2C_6H_3$)(COT″)] (**4**) appeared to be formed in an NMR-tube-scale reaction between [Ti(N-2,6-*i*$Pr_2C_6H_3$)Cl_2-$(py)_3$] and $Li_2[COT'']\cdot 1.8\,THF$, the product could not be cleanly isolated from larger scale reactions. The monomeric, asymmetrically substituted arylimido complex [Ti(N-2-*t*BuC_6H_4)(COT″)] (**5**) was prepared from the reaction between [Ti(N-2-*t*BuC_6H_4)$Cl_2(py)_3$] and $Li_2[COT'']\cdot 1.8\,THF$ in THF. Surprisingly, the analogous reaction between [Ti(N-2-*t*BuC_6H_4)$Cl_2(py)_3$] and $K_2[COT]$ did not produce any tractable products.

The most striking difference between the reaction products of $K_2[COT]$ and $Li_2[COT'']\cdot 1.8\,THF$ was observed with the moderately bulky arylimido derivative [Ti(N-2,6-$Me_2C_6H_3$)$Cl_2(py)_3$]. The reaction of this compound with $K_2[COT]$ in THF resulted in the formation of the crystallographically characterised (vide infra), dimeric imido-bridged complex $[Ti_2(\mu\text{-N-2,6-}Me_2C_6H_3)_2(COT)_2]$ (**6**) (Scheme 1).

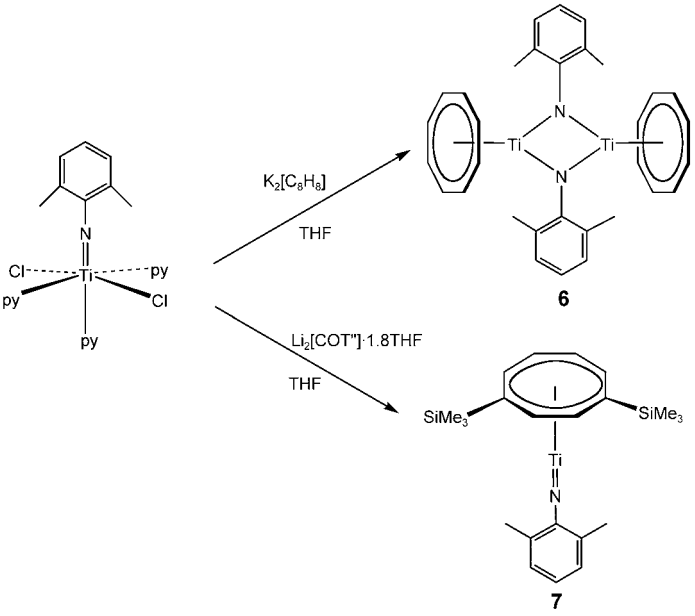

Scheme 1. Mono- and binuclear derivatives formed with the N-2,6-$Me_2C_6H_3$ ligand.

Unlike the lightly-coloured, highly soluble monomeric species **1**–**4**, this complex was dark red and only slightly soluble in most common organic solvents. Differences were also observed between the UV/Vis spectra of compounds **1** and **6**. The spectrum of compound **1** consisted of three principle transitions with the lowest energy one at 373 nm, whereas that of compound **6** contained four main transitions including a broad band at 686 nm.

The dimeric structure of **6** was maintained in solution as established from NOE experiements. A significant NOE enhancement was detected between the methyl protons of the 2,6-$Me_2C_6H_3$ aryl substituent and the protons of the COT

ring. This enhancement is only expected in a dimeric system in which the bent geometry around the bridging nitrogen atom brings the imido substituent into closer proximity to the COT ring. The solid-state structure of **6** indicates that the distance between the methyl protons of the 2,6-$Me_2C_6H_3$ aryl substituent and the protons of the COT ring can be as small as 2.35 Å, which is well within the range for observing NOE interactions. The corresponding distance between the methine proton of the isopropyl groups and the COT ring in the solid state of the monomeric species [Ti(N-2,6-$iPr_2C_6H_3$)(COT)] (**3**) is 3.64 Å. Given this large distance, it is not surprising that no NOE enhancement was observed between the methine proton and the COT ring in compound **3**. Presumably, the less sterically bulky 2,6-$Me_2C_6H_3$ imido substituent allows dimerisation to occur, whereas when the imido substituent is either *t*Bu or 2,6-$iPr_2C_6H_3$ steric factors prevent dimerisation.

The reaction of [Ti(N-2,6-$Me_2C_6H_3$)$Cl_2(py)_3$] with Li_2[COT″]·1.8THF yielded the monomeric orange complex [Ti(N-2,6-$Me_2C_6H_3$)(COT″)] (**6**) (Scheme 1). This complex is proposed to be monomeric based on its solubility, colour and a NOE experiment which showed that there was no enhancement between the methyl protons of the N-2,6-$Me_2C_6H_3$ imido substituent and the protons of the COT″ ring. In this case dimerisation is probably unfavourable due to the more sterically demanding COT″ ring.

The complexes [Ti(N-2,6-$iPr_2C_6H_3$)(COT)] (**3**), [Ti(N-2,6-$Me_2C_6H_3$)(COT″)] (**7**), [Ti(N-2-tBuC$_6H_4$)(COT″)] (**5**) and [Ti_2(μ-N-2,6-$Me_2C_6H_3$)$_2$(COT)$_2$] (**6**) could also be synthesised by *tert*-butylimido–aniline exchange by reaction of the appropriate *tert*-butylimido precursor (**1** or **2**) with the corresponding arylamine.[26,29] This method was problematic because the ligand exchange was slow even at elevated temperatures and it was difficult to remove any trace excess arylamine from the product. However, the ligand–exchange method was successfully utilised to synthesise the ring-unsubstituted phenyl-imido complex [Ti_2(μ-NPh)$_2$(COT″)$_2$] (**8**) [Eq. (2)]. Compound **8** was proposed to be dimeric on the basis of its solubility (insoluble in most common solvents), colour (dark red) and a significant NOE enhancement between the *ortho* and *meta* protons of the μ-NPh ligand and the protons of the COT″ ring. The nuclearity of this species supports the observation that as the steric bulk of the imido substituent is decreased, dimerisation becomes more favourable.

Solid-state structures: Crystals of monomeric [Ti(N*t*Bu)(COT)] (**1**) and [Ti(N-2,6-$iPr_2C_6H_3$)(COT)] (**3**) suitable for X-ray diffraction analysis were obtained by careful high-vacuum-tube sublimation. The solid-state structures of [Ti(N*t*Bu)(COT)] and [Ti(N-2,6-$iPr_2C_6H_3$)(COT)] are shown in Figure 1. Selected bond lengths and angles are presented in Table 1 and Table 2 together with those calculated by

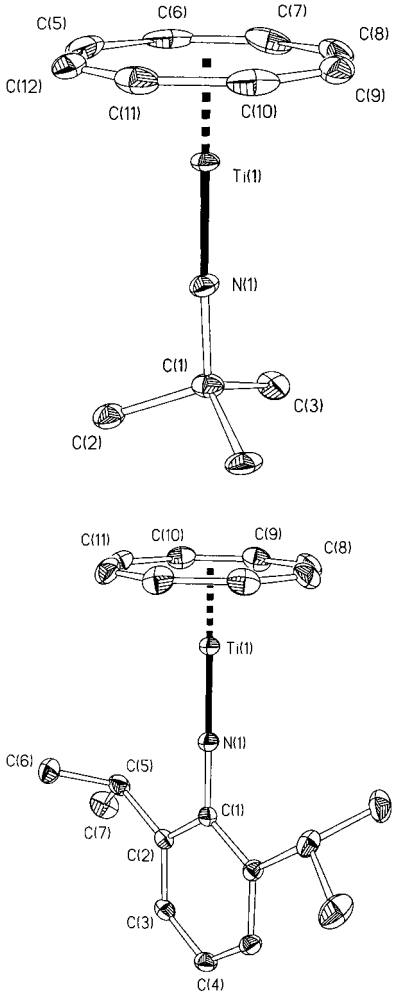

Figure 1. Displacement ellipsoid plots (30% probability) of [Ti(N*t*Bu)(COT)] (**1**, top) and [Ti(N-2,6-$iPr_2C_6H_3$)(COT)] (**3**, bottom). H atoms omitted for clarity.

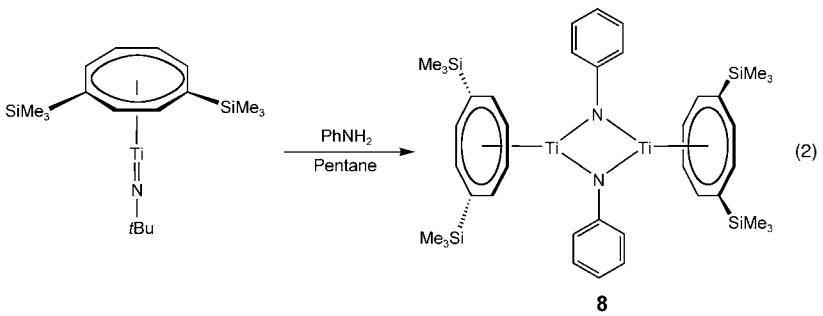

8

DFT analysis (vide infra). The pseudo-two-coordinate, ′pogo-stick′ or ′one-legged piano stool′ geometry observed for these complexes is unique in early transition-metal imido and cyclooctatetraenyl ligand chemistry.[1,31] A search of the Cambridge Structural Database for complexes of the type [Ti(η^8-COT)(L)$_n$] showed that

Table 1. Comparison between selected experimental and calculated bond lengths and angles for [Ti(N*t*Bu)(COT)] (**1**).

Bond lengths or angles	Experimental values [Å or °]	Calculated values [Å or °]
Ti–C ring	2.267(8)–2.290(8)	2.28
Ti(1)–N(1)	1.699(6)	1.69
N(1)–C(1)	1.45(5)	1.43
C–C ring	1.37(2)–1.44(2)	1.41
C–CH_3(*t*Bu)	1.51(1)–1.52(1)	1.52
C-C-C ring	133.9(9)–136.5(9)	135
C ring-Ti(1)-N(1)	125.9(3)–127.7(3)	126

Table 2. Comparison between selected experimental and calculated bond lengths and angles for [Ti(N-2,6-*i*$Pr_2C_6H_3$)(COT)] (**3**).

Bond lengths or angles	Experimental values [Å or °]	Calculated values [Å or °]
Ti–C ring	2.2778(16)–2.2885(16)	2.28
Ti(1)–N(1)	1.7217(18)	1.70
C–C ring (COT)	1.406(3)–1.413(3)	1.41
N(1)–C(1)	1.381(3)	1.37
C–C ring (aryl)	1.3918(19)–1.4209(18)	1.41
C(2)–C(5)	1.515(2)	1.50
C(5)–C(6)	1.529(3)	1.54
C(5)–C(7)	1.535(3)	1.54
C ring-Ti(1)-N(1) (COT)	125.9(3)-127.7(3)	126
Ti(1)-N(1)-C(1)	180	180
C-C-C ring (aryl)	118.61(14)-121.20(14)	119
C(1)-C(2)-C(5)	119.03(14)	121
C(3)-C(2)-C(5)	122.33(13)	121
C(2)-C(5)-C(6)	109.85(13)	111
C(2)-C(5)-C(7)	114.12(15)	111
C(6)-C(5)-C(7)	110.39(16)	112

the formal value of *n* is at least three.[32,33] Although there has previously been one report of imido complexes bearing cyclooctatetraenyl co-ligands, these complexes were neither monomeric nor structurally characterised.[27]

The Ti=N–*t*Bu and Ti···COT (ring centroid) distances of 1.699(6) and 1.369 Å in **1** are within the expected ranges for terminal titanium *tert*-butylimido and titanium(IV) η^8-cyclooctatetraenyl complexes, respectively.[32,33] The COT ring is planar and the complex is approximately C_s symmetric. The near-linearity of the Ti=N–*t*Bu angle (Ti(1)-N(1)-C(1) 177.1(5)°) is consistent with the imido ligand acting as a four-electron donor to the titanium center, giving the complex an overall metal valence-electron count of 16.

Compound **3** lies on a crystallographic two-fold rotation axis. As a consequence of the crystallographic symmetry, the ring centroid, Ti(1), N(1), and C(1) and C(4) atoms of the phenyl group are all required to be colinear and this axis is required to be exactly perpendicular to the COT plane. As for **1**, within experimental error the COT ring is planar and the Ti atom lies 1.35 Å from the best plane of this ligand. The Ti(1)–N(1) bond length in **3** of 1.7217(18) Å is consistent with typical literature values for titanium imido compounds with an arylimido substituent.[32,33] However, the Ti(1)–N(1) bond length in **3** is significantly longer (0.023(6) Å) than the corresponding bond length in **1**. This is probably the result of the electron-withdrawing nature of

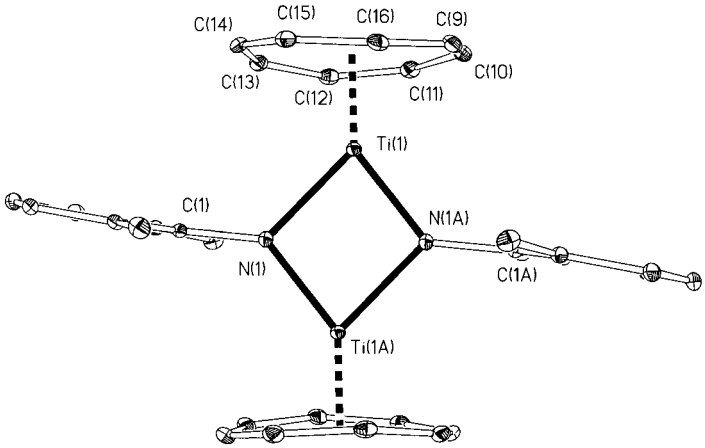

Figure 2. Displacement ellipsoid plot of [Ti_2(μ-N-2,6-$Me_2C_6H_3$)$_2$(COT)$_2$] (**6**) (15% probability). H atoms omitted for clarity.

aryl groups, compared to the inductively electron-donating alkyl group, and is well precedented.[26] Presumably, this causes a difference in the availability of the N_{imido} lone pair for donation to the metal.

X-ray diffraction quality crystals of dimeric [Ti_2(μ-N-2,6-$Me_2C_6H_3$)$_2$(COT)$_2$] (**6**) were grown from a saturated benzene solution at room temperature. The solid-state structure is shown in Figure 2. Selected distances and angles are given in Table 3, along with those calculated from DFT analysis (vide infra). The dimeric complex lies on a crystallographic centre of inversion and contains two pseudo-three coordinate titanium centres linked by two bridging N-2,6-$Me_2C_6H_3$ ligands, with the remainder of each metal coordination sphere consisting of an η^8-coordinated COT ring. The Ti···Ti

Table 3. Comparison between selected experimental and calculated bond lengths and angles for [Ti_2(μ-N-2,6-$Me_2C_6H_3$)$_2$(COT)$_2$] (**6**).

Bond lengths or angles	Experimental values [Å or °]	Calculated values [Å or °]
Ti(1)–N(1)	2.022(2)	1.95
Ti(1)–N(1A)	1.883(2)	1.92
Ti(1)–C(9)	2.380(3)	2.40
Ti(1)–C(10)	2.420(3)	2.44
Ti(1)–C(11)	2.357(3)	2.35
Ti(1)–C(12)	2.328(3)	2.31
Ti(1)–C(13)	2.427(3)	2.42
Ti(1)–C(14)	2.473(3)	2.46
Ti(1)–C(15)	2.397(3)	2.37
Ti(1)–C(16)	2.320(3)	2.32
N(1)–C(1)	1.411(3)	1.38
C(1)–C(2)	1.413(4)	1.41
N(1)-Ti(1)-N(1A)	81.82(10)	83
N(1)-Ti(1)-C(9)	156.25(10)	159
N(1 A)-Ti(1)-C(9)	97.66(10)	94
N(1)-Ti(1)-C(10)	169.60(11)	167
N(1)-Ti(1)-C(11)	137.30(10)	136
N(1)-Ti(1)-C(12)	107.62(10)	107
N(1)-Ti(1)-C(13)	89.9(1)	91
N(1)-Ti(1)-C(14)	87.78(9)	90
N(1)-Ti(1)-C(15)	99.67(10)	102
N(1)-Ti(1)-C(16)	124.32(10)	127

distance of 2.952 Å is not unusually short for a binuclear titanium(IV) complex, and similar distances have been observed in related species.[34–37] The Ti atom lies 1.54 Å from the centroid of the C_8 ring, which is significantly longer than in either of the monomeric compounds **1** and **3**, and the Ti···Ti···ring centroid angle is 173.5° suggesting some slippage of the ring. The bridging region of the complex is asymmetric, such that the Ti–N bond lengths are different (Ti(1)–N(1) 2.022(2), Ti(1)–N(1 A) 1.883(2) Å). Unsymmetrically bridging imides have previously been observed for several different transition-metal complexes and this effect increases π donation to the metal centre.[27,35,38]

The ligands of the complex are slightly distorted from their regular geometries. The dimethylphenyl group of the imide is bent slightly towards the Ti atom in the same asymmetric unit, so the Ti···Ti vector makes an angle of 84.7° with the best plane of the phenyl ring. Neither of the *ipso*-carbon atoms of the bridging μ-N-2,6-$Me_2C_6H_3$ ligands displays any interaction with the Ti centre in contrast to the significant interactions seen in similar zirconium,[27] samarium[38] and uranium[39–42] complexes. This lack of interaction could be for steric reasons or because titanium is smaller than these other metals. The COT ligand is distorted slightly from planarity towards a shallow saddle shape. This distortion presumably arises as a result of the strong *trans* influence of the imido nitrogen atoms. The carbon atoms of the COT ligand that are directly *trans* to the imido groups (namely C(10), C(13) and C(14)) show the largest Ti(1)–C_{ring} distances.

Density functional theory analysis of monomeric titanium imido compounds containing the cyclooctatetraenyl ligand: The electronic structure of [Ti(N*t*Bu)(COT)] (**1**) was compared with the electronic structures of [Ti(N*t*Bu)(COT′)] (**2**) and [Ti(N-2,6-*i*$Pr_2C_6H_3$)(COT)] (**3**). Density functional theory was used to model the related sets of compounds **1**, **2** and **3**. Geometry optimisations were performed assuming C_s symmetry for **1** and **2** and C_{2v} symmetry for **3**. Important calculated bond lengths and angles are compared with the experimental ones in Table 1 and Table 2. For compounds **1**, **2** and **3** a fragment analysis was performed in which the molecule was broken into a metal-ring fragment and an imido fragment.

As can be seen from Table 1 calculated bond lengths and angles for **1** generally showed good agreement. Although calculations were performed on **1** assuming the highest possible symmetry namely, C_s, for the purposes of this discussion the complex can be considered as having C_{8v} or $C_{\infty v}$ symmetry. This is because only the σ- and π-metal–ligand interactions of the nitrogen atom are important and consequently N*t*Bu can be thought of as a generic and cylindrically symmetric linear NR. It is also useful to characterise orbitals according to the σ, π and δ notation even though the actual symmetry of **1** is much lower than cylindrical. A MO diagram for **1** has been constructed in Figure 3.

There are three types of orbital interactions (π, σ and δ) for d^2 Ti(COT), which has local C_{8v} symmetry. The π orbi-

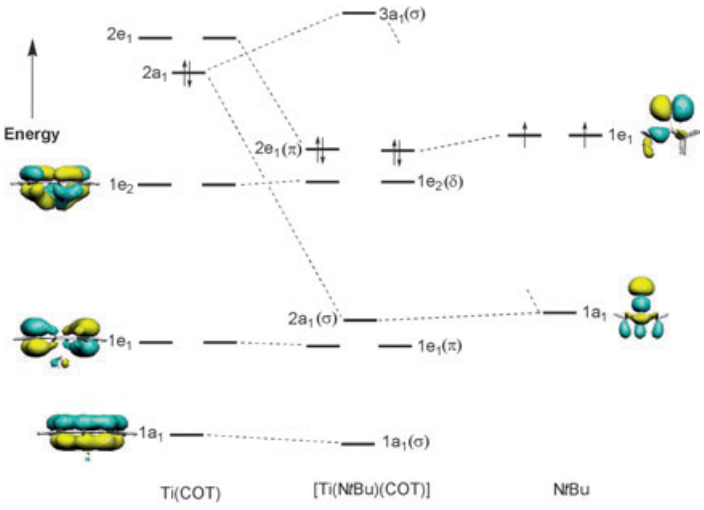

Figure 3. Partial molecular orbital diagram for [Ti(N*t*Bu)(COT)] (**1**).

tals of the carbocylic ring have a low-lying σ-symmetry orbital (a_1), a pair of π-symmetry orbitals (e_1) and a pair of δ-symmetry orbitals (e_2) all with respect to the metal–ring axis (z). Increasing the number of atoms in a carbocyclic ring decreases the energies of the π and δ molecular orbitals, but increases their occupancies.[43] Therefore, in the eight-membered COT ring the δ-symmetry orbitals become comparable in energy to the metal $d_{x^2-y^2}$ and d_{xy} orbitals, and the π-symmetry orbitals are lower in energy than the metal d_{xz} and d_{yz} orbitals. As a result, the predominant interaction in the binding of the COT ring to the titanium atom is through the δ orbitals (e_2), while the π orbitals are primarily non-bonding. The $2a_1$ and $2e_1$ orbitals of the Ti(COT) fragment are non-bonding orbitals and contain large contributions from the titanium $3d_{z^2}$ orbital for the $2a_1$ molecular orbital and from the degenerate titanium $3d_{xz}$ and $3d_{yz}$ orbitals for the $2e_1$ molecular orbitals. For the second fragment the imido ligand has a σ-type orbital ($1a_1$) and two π-type orbitals ($1e_1$) for bonding. The imido ligand forms a triple bond (σ^2, π^4-configuration) with the metal centre.

Isosurfaces for the $1e_2$, $1e_1$ and $2e_1$ orbitals and the $2a_1$ N-Ti σ-bonding orbital are shown in Figure 4. The $1e_2$ orbital can clearly be seen to be concerned with the bonding of the ring to the titanium atom, using the $3d_{x^2-y^2}$ and $3d_{xy}$ metal orbitals and the ring δ-symmetry orbitals. The $2e_1$ molecular orbital shows that the principle bonding of the imido group to the metal is through the two nitrogen 2p orbitals and $3d_{xz}$ and $3d_{yx}$ metal orbitals. Finally, the $1e_1$ orbital shows very little metal character, instead it is dominated by the ring π-symmetry orbitals and may be classed as metal–ligand non-bonding.

Good agreement was observed between the experimental and calculated bond lengths and angles for [Ti(N-2,6-*i*$Pr_2C_6H_3$)(COT)] (**3**) (Table 2). The bonding between the metal center and the C_8H_8 ring in complex **3** is similar to that described for complex **1**. However, differences were observed in the bonding of the imido ligand to the metal

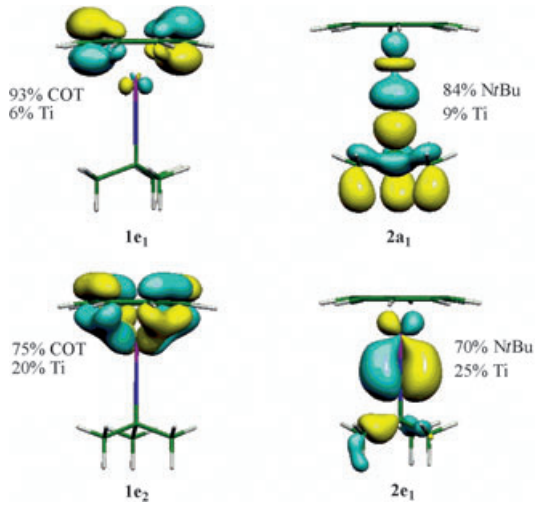

Figure 4. Selected isosurfaces of [Ti(N*t*Bu)(COT)] (**1**).

center. The pair of titanium–imido π-bonding orbitals ($2e_1$) which are degenerate in **1** are not degenerate in **3** (Figure 5). Instead, the titanium–imido π-bonding orbital

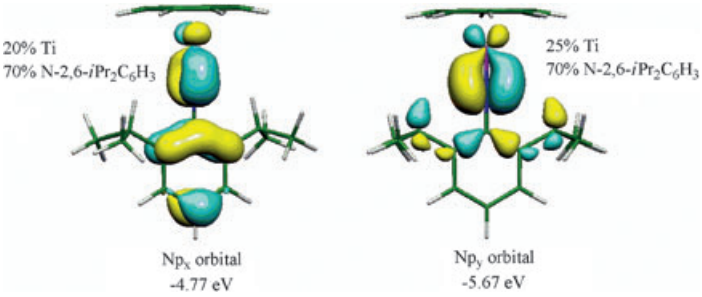

Figure 5. Isosurfaces and energies of Ti–N π-bonding orbitals in [Ti(N-2,6-iPr$_2$C$_6$H$_3$)(COT)] (**3**).

which is formed through the $2p_x$ orbital of the imido nitrogen is higher in energy than the corresponding π-bonding orbital which forms through the $2p_y$ orbital of the imido nitrogen atom. The loss of degeneracy arises because when the $2p_x$ orbital of the imido nitrogen forms a π-bond with the metal center there is also an unfavourable anti-bonding interaction between the $2p_x$ orbital of the nitrogen and the π-bonding orbitals of the aryl ring. As the $2p_y$ orbital of the imido nitrogen atom is orthogonal to the π-bonding orbitals of the aryl ring there is no anti-bonding interaction between these sets of orbitals when the $2p_y$ orbital of the imido nitrogen atom forms a π-bond with the metal centre.

The electronic structure of [Ti(N*t*Bu)(COT′)] (**2**) is extremely similar to that described for **1**. Fragment calculations indicated that the ordering and composition (determined by Mulliken population analysis) of the bonding orbitals in **1** and **2** were almost identical. From these calculations it is clear that although it has been shown experimentally that the introduction of $SiMe_3$ groups to the COT ring changes the solubility and steric properties of the complex, the presence of the $SiMe_3$ groups has almost no impact on the electronic properties of **2** compared with those of **1**.

General comparison of the bonding in the monomeric and dimeric complexes: To gain further insights into factors discriminating between monomeric and dimeric complexes, calculations were also performed on the models shown in Figure 6. The types of calculations performed and the energies of the models are summarised in Table 4.

The calculation performed on model compound **9** showed good agreement with the experimental bond lengths and angles for [Ti(N*t*Bu)(COT)] (**1**) (Table 5). Since the values are in excellent agreement with the experimental values, it is possible to consider **9** as a very good model for **1**.

For dimerisation of a linear cyclooctatetraenyl imido complex to occur, the ring centroid-Ti-N angle (α) must change

Table 4. Calculations performed on **1** and **9**–**14** and associated energies.

Structure	Calculation	Total energy [eV]
1	geometry optimisation	−182.545
9	geometry optimisation	−117.519
10	single point (angle α varied from 180–120°)	−114.981 (α = 120°)
11	single point (α = 137°, Ti-N-H = 180°)	−115.894
12	single point (α = 137°, Ti-N-H = 125°)	−116.064
13	geometry optimisation	−235.969
14	geometry optimisation	−363.806

Table 5. Comparison between selected experimental and calculated bond lengths and angles for [Ti(N*t*Bu)(COT)] (**1**) and [Ti(NH)(COT)] (**9**).

Bond lengths or angles	Experimental values [Å or °]	Calculated values [Å or °]
Ti–C ring	2.267(8)–2.290(8)	2.28
Ti(1)–N(1)	1.699(6)	1.68
C–C ring	1.37(2)–1.44(2)	1.41
C-C-C ring	133.9(9)–136.5(9)	135
C ring-Ti(1)-N(1)	125.9(3)–127.7(3)	126

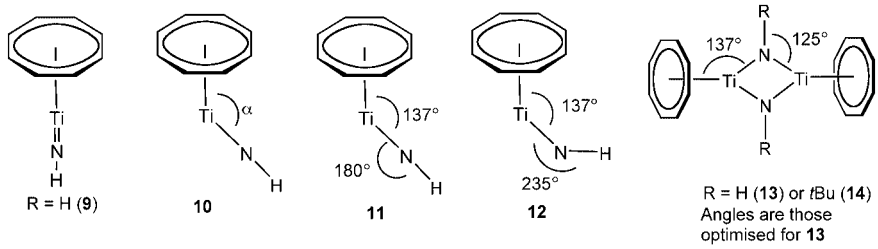

Figure 6. Model complexes **9**–**14** on which calculations were performed.

from linear (ca. 180°) to bent (ca. 120°, actually 137° in **6**) and the Ti=N–R angle must also decrease significantly. Linear transit calculations were first performed on the simplified [Ti(NH)(COT)] molecule to analyse the effect of changing the ring-Ti-N geometry from linear to bent (assuming C_{8v} symmetry when the ring-Ti-N angle was 180° and C_s symmetry otherwise). The variation in the orbital energies of **10** as a function of the bending angle α (180–120°) are shown in Figure 7a, while the change in total energy of

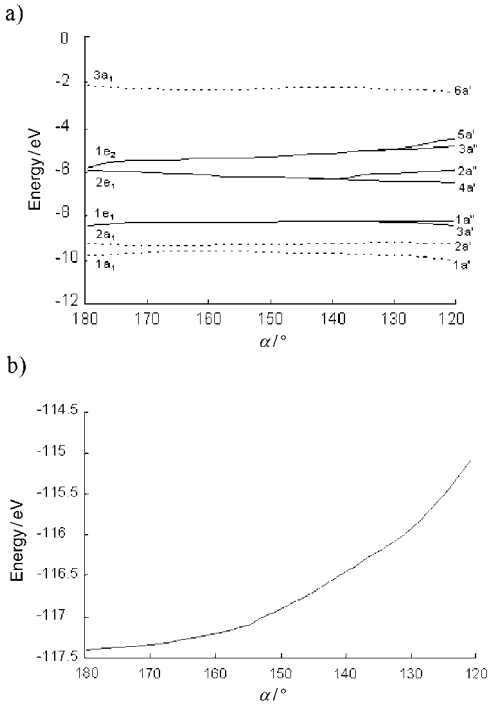

Figure 7. a) Variation in orbital energies of **10** as a function of the bending angle α (180–120°); b) change in total energy of **10** as a function of bending angle α (180 –120°).

10 as a function of the bending angle α(180–120°) is shown in Figure 7b. Figure 8 shows selected molecular orbitals of the linear molecule **9** and those of the corresponding bent molecule **10** with angle α of 120°.

The nitrogen–metal π interactions are stronger than the ring–metal interactions and so on bending the molecule this defines the z axis. There is a loss in overlap between the metal and the ring orbitals on bending which leads to a weakening of the interaction between the metal center and the cyclooctatetraenyl ring. This is a contributing factor to the destabilisation of the $1e_2$-derived orbitals 5a′ and 3a″. However, it is not the only one. On bending the molecule, strong unfavourable anti-bonding interactions develop between the ring orbitals and the nitrogen orbitals. As expected, the extent of this destabilisation increases as the molecule is bent further. This anti-bonding interaction explains the longer Ti···COT (ring centroid) distance in dimeric compound **6** compared to the monomeric compounds **1** and **3**.

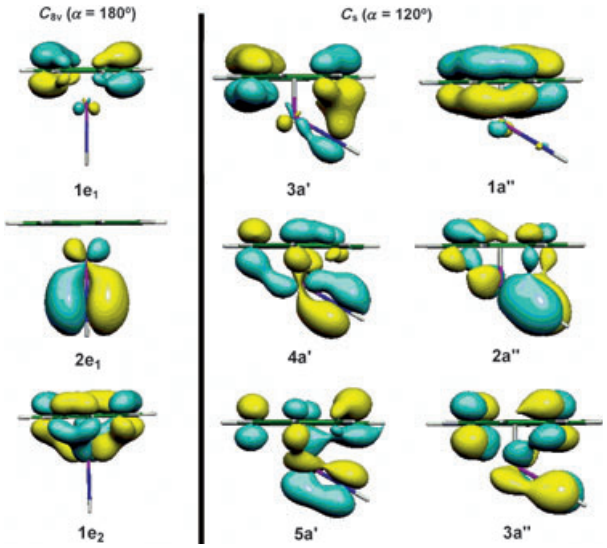

Figure 8. Selected MOs of [Ti(NH)(COT)] (**9**) with the corresponding MOs in **10** when $\alpha = 120$.

In contrast, the $2e_1$-derived orbitals (4a′ and 2a″) show a slight stabilisation when the molecule is bent. In this case, there are bonding interactions between the ring and the nitrogen 2p orbitals, as opposed to the anti-bonding interactions observed in the $1e_2$-derived orbitals. The $1e_1$-derived orbitals (3a′ and 1a″) show relatively little change in energy, which is expected since the $1e_1$ set are metal–ligand non-bonding orbitals, having mainly ligand character. Interestingly, there is little change in the energy of the LUMO on bending (3a′ going to 6a′). Since, this orbital stays low in energy the use of a good Lewis base could allow an 18-valence-electron adduct of bent **10** to be isolated if the shape changes favourably.[66]

Overall, the destabilisation of the $1e_2$-derived orbitals is greater than the stabilisation of the $2e_1$ orbital and so it is expected to be unfavourable to bend the molecule. This is clearly illustrated in Figure 7b, which shows the sharp increase in overall energy as angle α is increased.

Dimerisation of **9** or **1** leads to **13** or **14**, respectively (Figure 6). Geometry optimisation calculations were performed on **13** and **14** (Table 4). The ring-Ti-N and Ti=N-H angles obtained for **13** were used in single point calculations on models **11** (only the ring-Ti-N angle α changed from 180° in **9**) and then **12** (both ring-Ti-N and Ti=N-H angles perturbed). As expected, the energy of **11** is significantly greater than that of **9** (Table 4), whereas **12** is slightly more stable than **11**. It appears that the bending of the Ti=N-H angle in the distorted complex **11** has an energetically beneficial effect, at least when the imido N-substituent is a sterically non-demanding H atom. Despite the stabilisation gained on going from **11** (Ti=N-H = 180°) to **12** (Ti=N-H = 120°) the energies given in Table 4 show that overall conversion of **9** to **12** is an unfavourable process. However, from Table 4 it can be seen that the dimer **13** is 0.9 eV (86.8 kJ mol^{-1}) lower in energy than two hypothetical monomers **9**. This can be at-

tributed to the dimer gaining an extra σ bond. Since σ bonds are generally stronger than π bonds, the energy gained on dimerisation more than compensates for the reduced overlap and unfavourable interactions between the ring and the imido group. Although [Ti(NH)(COT)] is expected to exist as a dimer, the energies from the geometry optimisation calculations of **1** and **14** indicate that the [Ti(N*t*Bu)(COT)] monomer is approximately 1.23 eV (118.6 kJ mol^{-1}) lower in energy than the corresponding dimer even without taking into account the unfavourable entropy effects. Presumably, this is a result of the bulky *tert*-butyl groups of the imido ligand interacting with both rings in the dimer. These calculations clearly support the experimental results which indicate that formation of a monomer is more likely to be favoured as the steric bulk on the imide is increased.

Density functional theory analysis of [Ti_2(μ-N-2,6-$Me_2C_6H_3$)$_2$(COT)$_2$] (6): The electronic structure of [Ti_2(μ-N-2,6-$Me_2C_6H_3$)$_2$(COT)$_2$] (**6**) was compared with those of **1**, **2** and **3**. DFT was used to model compound **6** and a geometry optimisation was performed on **6** with no symmetry restrictions. Important calculated bond lengths and angles are compared with the experimental ones in Table 3. A fragment analysis was performed where **6** was broken into two metal–ring fragments and two imido fragments.

The geometry optimisation of **6** showed that there was a discrepancy between the optimised bond lengths and angles and the experimental values especially with regard to the central $Ti_2(\mu\text{-}N)_2$ unit of **6**, but otherwise there was good agreement, as shown in Table 3. The degree of asymmetry present in the $Ti_2(\mu\text{-}N)_2$ core can be quantified by considering the difference between the distances Ti(1)–N(1) and Ti(1)–N(1A). This difference was considerably larger in the experimental structure (0.139(3) Å) than in the calculated structure (0.03 Å). A linear transit calculation was performed to examine the changes in the total energy of **6** when the geometry of the molecule was optimised at different Ti(1)–N(1) bond lengths. For computational simplicity the calculations were performed assuming the molecule had C_{2h} symmetry. Figure 9 shows the changes in energy of [Ti_2(μ-N-2,6- $Me_2C_6H_3$)$_2$(COT)$_2$] as the Ti(1)–N(1) bond length is changed.

This calculation indicates that there is almost no change in the overall energy of [Ti_2(μ-N-2,6-$Me_2C_6H_3$)$_2$(COT)$_2$] (**6**) as the Ti(1)–N(1) is changed from 1.85 to 1.95 Å. The Ti(1)–N(1) bond length is clearly 'soft' in nature and it is reasonable to conclude that the differences between the calculated and experimental structures are due to crystal packing forces.

The major difference between the electronic structures of monomeric complexes such as **1** and that of **6** relate to the composition of the HOMO(s). In [Ti(N*t*Bu)(COT)], the HOMOs represent π bonds between nitrogen 2p orbitals and metal orbitals of suitable symmetry. However, as a result of the change of geometry around the imido nitrogens in **6**, there is poor overlap between one of the linear combinations of the nitrogen 2p orbitals and the metal $3d_{z^2}$ orbital. Therefore, the HOMO in **6** is non-bonding and consists mainly of nitrogen p orbital character. Isosurfaces for the HOMO and LUMO of **6** are shown in Figure 10.

In both **1** and **6** the LUMO has mainly metal d character. However, as a result of the differences in compositions of the HOMO, the energy gap between the HOMO and LUMO in [Ti(N*t*Bu)(COT)] (**1**) is 3.29 eV (317 kJ mol^{-1}), whereas the corresponding gap in [Ti_2(μ-N-2,6-$C_6H_3Me_2$)$_2$(COT)$_2$] (**6**) is 1.14 eV (110 kJ mol^{-1}). Although the difference in energy between the HOMO and LUMO can not be used to predict the energies of transitions in the UV spectrum, the difference between the sizes of the HOMO–LUMO gap in **1** and **6** are consistent with the observation of a transition at lower energy in the UV/Vis spectrum of **6** compared with **1**. This difference in the size of the HOMO–LUMO gap probably explains why dimeric complexes absorb more in the visible region of the spectrum and tend to be very dark in colour, while monomeric complexes

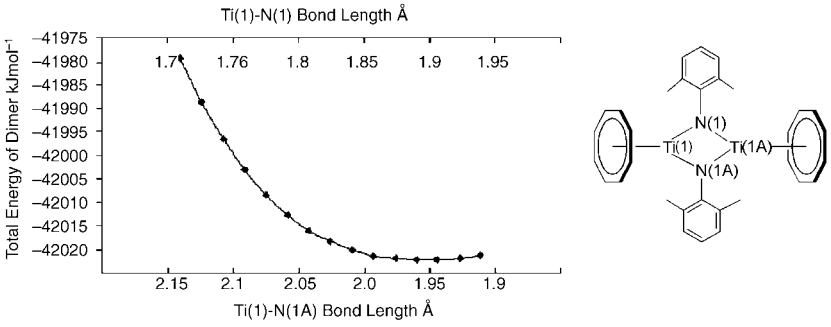

Figure 9. Variation in total energy of [Ti_2(μ-N-2,6-$Me_2C_6H_3$)$_2$(COT)$_2$] (**6**) against Ti(1)–N(1) and Ti(1)–N(1A) bond lengths.

Figure 10. Isosurfaces of selected molecular orbitals of [Ti_2(μ-N-2,6-$Me_2C_6H_3$)$_2$(COT)$_2$] (**6**).

absorb almost entirely in the near UV with a tail in visible region of the spectrum and are paler in colour (yellow or orange).

Photoelectron spectroscopy: The gas-phase He(I) photoelectron (PE) spectra of [Ti(N*t*-Bu)(COT)] (**1**), [Ti(N*t*Bu)-(COT′′)] (**2**) and [Ti(N-2,6-*i*Pr$_2$C$_6$H$_3$)(COT)] (**3**) are shown in Figure 11 and vertical ionisation energies (IEs) are summarised in Table 6. Their assignment is made relatively straightforward by comparison with related imido and cyclooctatetraenyl compounds.[44,45] The apparent paucity of low ionisation energy bands for [Ti(N*t*Bu)(COT)] (**1**) is explained by the fact that the 1e$_2$ ionisation of the Ti-COT ring δ-bonding orbitals overlaps with the 2e$_1$ ionisation of the Ti–N π bonds producing a complex band centred at 8 eV with two distinct maxima. Band C at 10.91 eV may be assigned to the 1e$_1$ ionisation of the COT ring orbitals. The relative increase in intensity of bands A and B relative to C in the He II spectrum (not shown here[30]) indicates that the 1e$_2$ and 2e$_1$ orbitals that give rise to bands A and B have significant metal character. Mulliken population analysis of the ground state structure of [Ti(N*t*Bu)(COT)] (**1**) gives the Ti contribution to the 2e$_1$ and 1e$_2$ orbitals as 28% and 22%, while that of the 1e$_1$ is estimated as 8%. This is consistent with the intensity increase of bands A and B relative to C as the photon energy is increased and supports the molecular orbital diagram that was proposed in Figure 3.

Table 6. Experimental and calculated vertical IEs (eV) for **1**, **2** and **3**. C_s symmetry was assumed for **1** and **2** and C_{2v} for **3**. Ion state calculations that failed to converge are marked with an asterisk.

	1 exptl	**1** calcd	**2** exptl	**2** calcd	**3** exptl	**3** calcd
Ti–N π	7.78 (A)	7.70 (A′)	7.47 (A)	* (A′)	7.00 (A)	6.83 (B_1)
		7.69 (A″)		7.29 (A″)		7.85 (B_2)
Ti–COT δ	8.05 (B)	7.85 (A′)	7.87 (B)	7.42 (A′)	7.98 (B)	7.72 (A_2)
		7.86 (A″)		7.55 (A″)	7.95 (A_1)	
aryl π						7.46 (A_2)
					9.64 (C)	9.33 (B_1)
COT e$_1$	10.91 (C)	* (A′)				
		10.60 (A″)				

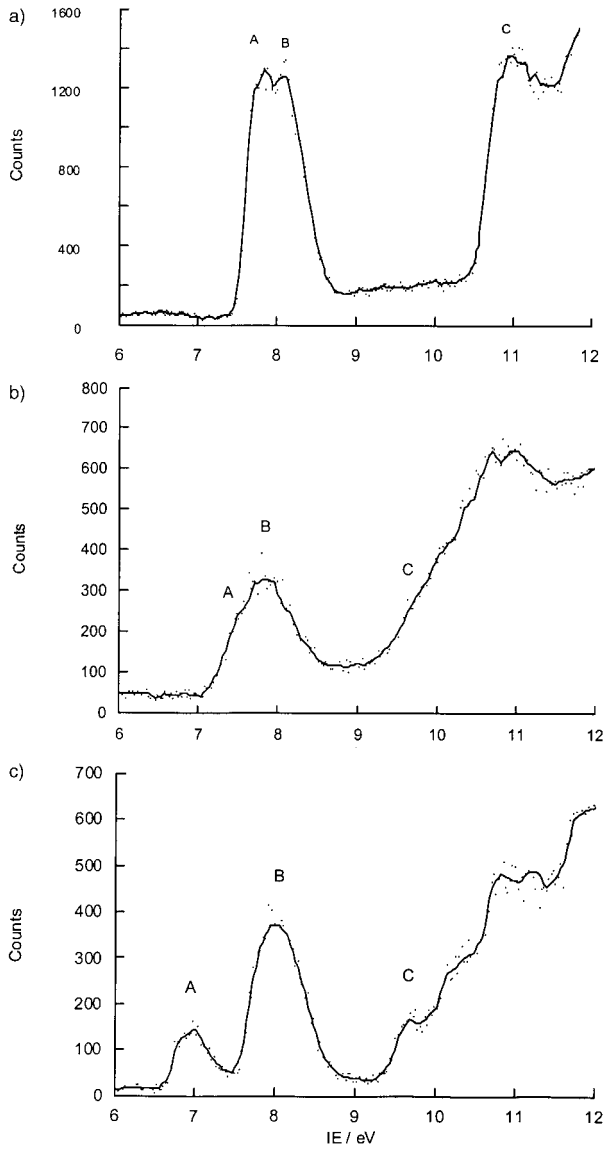

Figure 11. Gas-phase He(I) PE spectra of a) [Ti(N*t*Bu)(COT)] (**1**); b) [Ti(N*t*Bu)(COT′′)] (**2**), and c) [Ti(N-2,6-*i*Pr$_2$C$_6$H$_3$)(COT)] (**3**).

The PE spectrum of [Ti(N*t*Bu)(COT′′)] (**2**) has a very similar low energy structure, though in this case only one vertical IE (B) and a shoulder (A) can be distinguished. The IE is lower than for **1** reflecting the electron donating effect of the SiMe$_3$ substituents. The higher energy bands, C and above, in this case are associated with SiMe$_3$ ionisations, which overlay the ring 1e$_1$ π band.

The PE spectrum of [Ti(N-2,6-*i*Pr$_2$C$_6$H$_3$)(COT)] (**3**) differs from those of **1** and **2** in the low-energy region. The first band, A, is separated from the principal low-energy band B by almost 1 eV. Band B occurs in a similar position to the low-energy bands A and B of **1**. Assignment of the IE bands in **3** is most easily discussed while considering the calculated IEs. Table 5 gives both experimental and calculated IEs for **1**–**3**.

In the low IE region, agreement is generally very good. All three calculations suggest that a Ti–N π ionisation is the lowest in energy. The Ti–COT δ ionisations lie very close in energy to the Ti–N π ionisation but in all three complexes are predicted to occur at slightly higher energy. For **1**, though the symmetry is only C_s the effective degeneracy of the calculated IE for the two Ti–N π orbitals and also for the two Ti–COT δ orbitals demonstrates that the assumption of pseudo-C_{8v} is legitimate. For **2** the two Ti–COT′′ δ IEs are separated by 0.13 eV, due to ring substitution, which accounts for the lack of structure in the band. For **3**, band A

may be assigned to an out of phase combination of the Ti–N π-bonding electrons with an aryl π orbital (see Figure 5). Band B contains, in addition to the orthogonal Ti–N π-bonding ionisation and the Ti–COT δ band, the other aryl ionisation. The IE calculated for the in-phase combination of the aryl π orbital with the Np π orbital is 9.33 eV and may be identified with band C.

An interesting comparison may be made with the 17-valence-electron, d^1 compound [Ti(COT)(η^5-C_5Me_5)].[44] In the PE spectrum of this compound there is an additional low-lying ionisation band of the extra d electron at 5.28 eV, but the e_2 and $2e_1$ bands are also found to be coincident with a maximum at 7.54 eV. Furthermore, the $1e_1$ band lies at 10.5 eV which is of a very similar energy to that for [Ti(N*t*Bu)(COT)] (**1**). Thus we may conclude that the cyclopentadienylimido analogy[45] holds for these compounds and that the *tert*-butylimido ligand is electronically similar to the pentamethylcyclopentadienyl ligand though it provides one less electron.

General comparison of bonding in 'pogo-stick' complexes: In the early 1990s Bergman and co-workers reported the late transition metal 'pogo-stick' complexes [Os(N*t*Bu)(η^6-C_6Me_6)][29] and [Ir(N*t*Bu)(η^5-C_5Me_5)].[28] Many years earlier the Group 10 'pogo-stick' complex [Ni(NO)(η^5-C_5H_5)] (**14**) had been reported by King et al.[46] The geometry of these 18-electron complexes is similar to that of **1** and so a DFT-based comparison between the bonding in early transition metal 'pogo-stick' and late transition metal 'pogo-stick' complexes has been performed. For computational simplicity [Os(N*t*Bu)(η^6-C_6Me_6)] and [Ir(N*t*Bu)(η^5-C_5Me_5)] were modelled as [Os(N*t*Bu)(η^6-C_6H_6)] (**15**) and [Ir(N*t*Bu)(η^5-C_5H_5)] (**16**), respectively. DFT analyses have previously been performed on **14**[47,48] and the bonding in compounds **15** and **16** studied by using extended Hückel MO theory.[45] However, our present DFT analyses were performed on **14**, **15** and **16** for the purpose of directly comparing the bonding in these compounds with the bonding in compound **1**. Geometry optimisations were performed on **14**, **15** and **16** assuming C_{5v}, C_{3v} and C_s symmetry, respectively. In addition, fragment analyses were performed in which **14** was broken into a metal–ring fragment and a nitrosyl fragment, and **15** and **16** were broken into a metal–ring fragment and an imido fragment.

The bonding in the closely related compounds [Os(N*t*Bu)(η^6-C_6H_6)] (**15**) and [Ir(N*t*Bu)(η^5-C_5H_5)] (**16**) is extremely similar. As described earlier for the COT ring, the C_6H_6 and C_5H_5 rings have a low-lying σ-symmetry orbital (a_1), a pair of π-symmetry orbitals (e_1) and a pair of δ-symmetry orbitals (e_2) all with respect to the metal–ring axis. However, in the smaller carbocyclic rings the δ-symmetry orbitals (e_2) are raised in energy and as a result there is no significant interaction between the metal $d_{x^2-y^2}$ and d_{xy} orbitals and the δ-symmetry orbitals of the carbocyclic rings in **15** and **16**. (It should also be noted that the size of the COT ring compared to a C_6H_6 or C_5H_5 ring allows for better orbital overlap between the relevant metal d orbitals and the ring δ-symmetry orbitals). In both compounds **15** and **16** the metal $d_{x^2-y^2}$ and d_{xy} orbitals are primarily non-bonding. Instead, the predominant metal–ring bonding interaction occurs between the metal d_{xz} and d_{yz} orbitals and the π-symmetry orbitals (e_1) of the carbocyclic ring. The imido ligand also provides a set of π-symmetry orbitals (e_1) for bonding with the metal d_{xz} and d_{yz} orbitals. The mixing of the π-symmetry orbitals (e_1) of both ligands and the metal $5d_{xz}$, $5d_{yz}$ and $6p_x$ and $6p_y$ orbitals results in three sets of MOs of e_1 symmetry. Isosurfaces for the $1e_1$, $2e_1$ and $3e_1$ MOs of [Os(N*t*Bu)(η^6-C_6H_6)] (**15**) are shown in Figure 12a. The $3e_1$ orbital which is anti-bonding with respect to both the metal–imide and metal–ring π bonds is the LUMO in **15**.

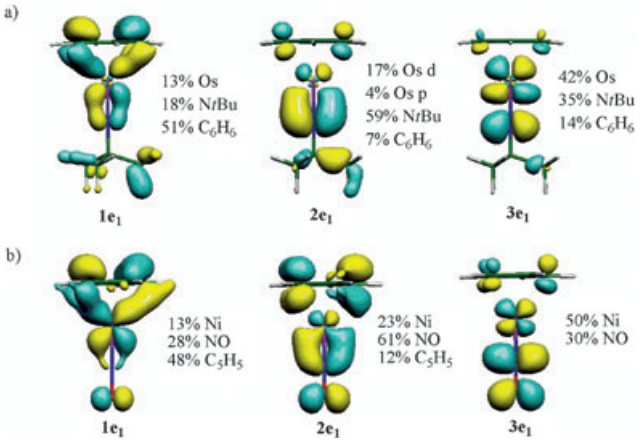

Figure 12. a) Selected isosurfaces of [Os(N*t*Bu)(η^6-C_6H_6)] (**15**); b) selected isosurfaces of [Ni(NO)(η^5-C_5H_5)] (**14**).

This mixing of the π-symmetry orbitals between the ligands is in direct contrast to the partitioning of the metal orbitals that occurs in compound **1**, where only the imido ligand interacts with the metal d_{xz} and d_{yz} orbitals and the metal $d_{x^2-y^2}$ and d_{xy} orbitals interact with the carbocyclic ring. The other major difference between the bonding in compounds **15** and **16** and compound **1** is that the metal d_{z^2} orbitals in both **15** and **16** are occupied and are the HOMO whereas the metal d_{z^2} orbital is unoccupied and the LUMO in **1**. The total metal-valence-electron count for the osmium and iridium complexes is 18 compared to 16 for compound **1**.

The bonding between the C_5H_5 ring and the metal centre in [Ni(NO)(η^5-C_5H_5)] (**14**) is similar to that described for the iridium and osmium complexes and consistent with previous descriptions of the bonding between M–Cp and M–arene fragments.[43] The predominant metal–ring bonding interaction occurs between the metal d_{xz} and d_{yz} orbitals and the π-symmetry orbitals (e_1) of the carbocyclic ring to form a bonding as well an anti-bonding pair of occupied MOs of e_1 symmetry. The only orbitals of the NO fragment which interact with the Ni(η^5-C_5H_5) fragment are the nitrogen–oxygen π anti-bonding orbitals which also have e_1 symmetry. The π anti-bonding orbitals of the NO fragment interact

with the higher lying anti-bonding e_1 pair of MOs of the Ni(η^5-C_5H_5). This results in the strengthening of the metal–ring bond because the ring–metal anti-bonding orbital is now delocalised onto the NO fragment. Iso-surfaces for the $1e_1$, $2e_1$ and $3e_1$ MOs of [Ni(NO)(η^5-C_5H_5)] (**14**) are shown in Figure 12b. As with compounds **15** and **16** the $3e_1$ orbital is anti-bonding with respect to both the metal–nitrosyl and metal–ring π bonds and is the LUMO in **14**.

In comparing the bonding in compounds **1**, **14**, **15** and **16** it is clear that the crucial factor in determining which metal orbitals interact with the carbocyclic ring is the number of carbon atoms in the carbocyclic ring. The Group 10 complex [Ni(NO)(η^5-C_5H_5)] (**14**) is interesting because the nitrosyl ligand interacts with a metal–ring anti-bonding orbital as opposed to the imido ligand which interacts with a metal–ring bonding orbital in compounds **15** and **16** and a non-bonding metal based orbital in compound **1**. Therefore the introduction of the second ligand increases the strength of the metal–ring bonding in **14**, weakens the strength of the metal–ring bonding in **15** and **16** and does not significantly affect the strength of the metal–ring bonding in **1**. Only compound **1** has a completely metal-based LUMO and this probably indicates that nucleophiles are more likely to react at the 16-valence-electron metal centre in **1** than with compounds **14**, **15** or **16**. It has previously been shown that [2 + 2] cycloadditions occur between the metal–N*t*Bu fragments in **15** and **16** and unsaturated substrates such as isocyanates and isocyanides.[28,29] Given the similarity in the bonding between the metal and N*t*Bu fragments in compounds **15**, **16** and **1**, we predict that compound **1** will also undergo cycloaddition reactions with unsaturated substrates.

Conclusion

In conclusion, we have firmly established a new class of early transition-metal cyclooctatetraenylimido complexes through structural, spectroscopic and theoretical studies. The steric bulk on both the imido substituent and cyclooctatetraenyl ring are crucial factors in determining the nuclearity of the product. Increasing the steric bulk of either ligand increases the likelihood of forming a monomeric complex. Density functional theory analysis indicates that the most striking aspect of the metal–ligand bonding orbitals is that binding to the imido group is primarily through σ and π interactions, whereas that to the COT or COT″ ring is almost exclusively through δ-symmetry orbitals. Recent preliminary studies suggest that the Ti=NR linkages in complexes of the type [Ti(NR)(COT)] are reactive towards a range of organic substrates. Our work in this area and syntheses of other early transition-metal cyclooctatetraenylimido complexes is continuing.

Experimental Section

General methods and instrumentation: All manipulations were carried out using standard Schlenk line or dry-box techniques under an atmosphere of argon or dinitrogen. Solvents were pre-dried over activated 4 Å molecular sieves and were refluxed over appropriate drying agents under a dinitrogen atmosphere and collected by distillation. Deuterated solvents were dried over appropriate drying agents, distilled under reduced pressure, and stored under dinitrogen in Teflon valve ampoules. NMR samples were prepared under dinitrogen in 5-mm Wilmad 507-PP tubes fitted with J. Young Teflon valves. ^{1}H and ^{13}C spectra were recorded on Varian Unity Plus 300 and Varian Mercury spectrometers. ^{1}H and ^{13}C assignments were confirmed when necessary with the use of NOE, and two-dimensional ^{1}H–^{1}H and ^{13}C–^{1}H NMR experiments. All spectra were referenced internally to residual protio-solvent (^{1}H) or solvent (^{13}C) resonances and are reported relative to tetramethylsilane ($\delta = 0$ ppm). Chemical shifts are quoted in δ (ppm) and coupling constants in hertz. Infrared spectra were prepared as Nujol mulls between NaCl or KBr plates and were recorded on Perkin-Elmer 1600 and 1700 series spectrometers. Infrared data are quoted in wavenumbers (cm^{-1}). UV absorption spectra were recorded on a Perkin-Elmer Lambda 19 UV-visible spectrophotometer. Molar absorption coefficients are reported in L mol^{-1} cm^{-1}. Mass spectra were recorded by the mass spectrometry service of the University of Oxford's Inorganic Chemistry Laboratory. Combustion analyses were recorded by the analytical services of the University of Oxford's Inorganic Chemistry Laboratory or by Mikroanalytisches Labor Pascher.

Despite numerous attempts, low %C analyses were consistently found for all of the new compounds even after purification by tube sublimation or recrystallisation. This is attributed to incomplete combustion. X-ray crystal structures of the key compounds **1**, **3** and **6** have been reported and several compounds give well-defined molecular ions in their high-resolution EI mass spectra. All new compounds were spectroscopically pure by NMR spectroscopy.

PE spectra were measured by using a Helectros 0078 spectrometer with a He discharge lamp capable of producing both He I and He II spectra. The spectrometer was interfaced with an Atari processor, which enabled spectral acquisition by repeated scans. The samples were calibrated by using He, Xe, and N_2 and band intensities were estimated by using the Gaussian fitting program available in the IGOR program suite. Band positions and widths were obtained by a free fit to the He I spectra and were maintained at the same IE and proportionate widths for the lower resolution He II spectra.

Density functional calculations were carried out using the Amsterdam Density Functional program suite ADF 2002.02.[49] Scalar relativistic corrections were included via the ZORA method.[50–54] The generalised gradient approximation was employed, using the local density approximation of Vosko, Wilk, and Nusair[55] together with non-local exchange correction by Becke[56,57] and non-local correlation corrections by Perdew.[58] TZ2P basis sets were used with triple-accuracy sets of Slater type orbitals and two polarisation functions added to the main group atoms. The cores of the atoms were frozen up to 1s for C and N, 2p for Ti, Si and Ni and 4f for Ir and Os. Vertical ionisation energies (IE) were estimated by calculating the energy of the molecular ions in their ground or excited states with the optimised geometry of the molecule. The IEs were found by the energy differences from that of the parent molecule.

Literature preparations: [Ti(N*t*Bu)Cl_2(py)$_3$],[26] [Ti(N-2,6-$Me_2C_6H_3$)Cl_2(py)$_3$],[26] [Ti(N-2,6-*i*$Pr_2C_6H_3$)Cl_2(py)$_3$],[26] [Ti(N-2-*t*BuC_6H_4)Cl_2(py)$_3$],[21] K_2[COT],[59] and Li_2[COT″]·1.8THF[60] were prepared by using literature methods.

[Ti(N*t*Bu)(COT)] (1): To a stirred solution of [Ti(N*t*Bu)Cl_2(py)$_3$] (4.00 g, 9.36 mmol) in THF (70 mL) at −50 °C was added a solution of K_2[COT] (1.71 g, 9.36 mmol) in THF (30 mL) over 15 min. The reaction mixture was warmed to room temperature and stirred for 16 h, during which time it became dark brown. The volatiles were removed under reduced pressure and the residue extracted into Et_2O (3 × 30 mL) and filtered. The volatiles were removed again and the residue was washed with pentane (3 × 15 mL) and dried in vacuo. This afforded **1** as a light brown/yellow

solid. Analysis by ^{1}H NMR spectroscopy indicated that the sample was sufficiently pure for further studies. Yield: 1.40 g (67%). Spectroscopically pure samples were obtained by tube sublimation (100–110°C, 5×10^{-4} mbar). Yellow crystals suitable for X-ray diffraction were obtained by tube sublimation (100–110°C, 5×10^{-4} mbar).

^{1}H NMR data (C_6D_6, 300.0 MHz, 298 K): $\delta=6.69$ (s, 8H; C_8H_8), 0.71 ppm (s, 9H; N*t*Bu); ^{13}C-{^{1}H} NMR data (C_6D_6, 75.5 MHz, 298 K): $\delta=95.6$ (C_8H_8), 71.1 (N*C*Me$_3$), 32.9 ppm (NC*Me*$_3$); IR data (NaCl plates, Nujol mull): $\tilde{\nu}=1260$ (sh, s), 1234 (sh, s), 1092 (br, s), 1020 (br, s), 800 (s), 730 cm^{-1} (m); UV data (benzene): $\lambda_{max}=280$ (2044), 328 (1361), 373 nm (1042); EI-MS: *m/z*: 223 ([*M*]$^+$), 209 ([*M*−Me]$^+$), 167 ([*M*−N*t*Bu]$^+$), 104 ([COT]$^+$), 58 ([N*t*Bu]$^+$); HR EI-MS for [Ti(N*t*Bu)(COT)]; found (calcd for $C_{12}H_{17}NTi$) *m/z*: 223.0840 (223.0840); elemental analysis calcd (%) for $C_{12}H_{17}NTi$: C 64.6, H 7.7, N 6.3; found: C 63.6, H 7.4, N 6.1.

[Ti(N*t*Bu)(COT′)] (2): To a stirred solution of [Ti(N*t*Bu)Cl$_2$(py)$_3$] (1.80 g, 4.20 mmol) in THF (40 mL) at −50°C was added a solution of Li$_2$[COT′]·1.8THF (1.65 g, 4.20 mmol) in THF (20 mL) over 15 min. The reaction mixture was warmed to room temperature and stirred for 16 h, during which time it became dark brown. The volatiles were removed under reduced pressure and the residue extracted into pentane (3× 15 mL) and filtered. Subsequent removal of the volatiles under reduced pressure afforded **2** as a light brown solid. Analysis by ^{1}H NMR spectroscopy indicated that the sample was sufficiently pure for further studies. Yield: 0.83 g (54%). Spectroscopically pure samples were prepared by tube sublimation (130°C, 5×10^{-4} mbar).

^{1}H NMR data (C_6D_6, 300.0 MHz, 298 K): $\delta=7.29$ (s, 2H; 2- and 3-$C_8H_6(SiMe_3)_2$), 7.15 (m, 2H; 5- and 8-$C_8H_6(SiMe_3)_2$), 6.89 (m, 2H; 6- and 7-$C_8H_6(SiMe_3)_2$), 0.66 (s, 9H; N*t*Bu), 0.55 ppm (s, 18H; SiMe$_3$); ^{13}C{^{1}H} NMR data (C_6D_6, 75.5 MHz, 298 K): $\delta=105.6$ (1- and 4-$C_8H_6(SiMe_3)_2$), 102.0 (2- and 3-$C_8H_6(SiMe_3)_2$), 99.8 (5- and 8-$C_8H_6(SiMe_3)_2$), 97.8 (6- and 7-$C_8H_6(SiMe_3)_2$), 70.8 (N*C*Me$_3$), 33.1 (NC*Me*$_3$), 0.7 ppm (SiMe$_3$); IR (Nujol mull, NaCl plates): $\tilde{\nu}=1250$ (sh, s), 1236 (s), 1044 (m), 836 (s), 754 cm^{-1} (m); EI-MS: *m/z*: 367 ([*M*]$^+$), 352 ([*M*−Me]$^+$), 248 ([COT′]$^+$), 73 ([SiMe$_3$]$^+$); HR EI-MS for [Ti(N*t*Bu)(COT′)]: found (calcd for $C_{18}H_{33}Si_2NTi$): *m/z*: 367.1631 (367.1631); elemental analysis calcd (%) for $C_{18}H_{33}Si_2NTi$: C 58.9, H 9.1, N 3.8; found: C 58.2, H 9.0, N 3.7.

[Ti(N-2,6-*i*Pr$_2$C$_6$H$_3$)(COT)] (3): To a stirred solution of [Ti(N-2,6-*i*Pr$_2$C$_6$H$_3$)Cl$_2$(py)$_3$] (1.52 g, 2.80 mmol) in THF (40 mL) was added a solution of K$_2$[COT] (0.51 g, 2.80 mmol) in THF (20 mL). The reaction mixture was stirred for 16 h, during which time it became dark brown. The volatiles were removed under reduced pressure and the residue extracted into Et$_2$O (2×25 mL) and filtered. The volatiles were removed again and the residue washed with pentane (2×25 mL) and dried in vacuo. This afforded **3** as an orange solid. Analysis by ^{1}H NMR spectroscopy indicated that the sample was sufficiently pure for further studies. Yield: 0.53 g (58%). Spectroscopically pure samples were obtained by tube sublimation (170–180°C, 5×10^{-4} mbar). Orange crystals suitable for X-ray diffraction were obtained by tube sublimation (170–180°C, 5×10^{-4} mbar).

^{1}H NMR data (C_6D_6, 300.0 MHz, 298 K): $\delta=7.29$ (d, $^3J=7.5$ Hz, 2H; *meta*-N-2,6-*i*Pr$_2$C$_6$H$_3$), 7.15 (1H, partially obscured t, *para*-N-2,6-*i*Pr$_2$C$_6$H$_3$, coupling unresolved), 6.69 (s, 8H; C_8H_8), 3.22 (sept, $^3J=6.9$ Hz, 1H; C*H*Me$_2$), 1.21 ppm (d, $^3J=6.9$ Hz, 12H; CH*Me*$_2$); ^{13}C{^{1}H} NMR data (C_6D_6, 75.5 MHz, 298 K): $\delta=159.9$ (*ipso*-N-2,6-*i*Pr$_2$C$_6$H$_3$), 139.3 (*ortho*-N-2,6-*i*Pr$_2$C$_6$H$_3$), 121.7 (*meta*-N-2,6-*i*Pr$_2$C$_6$H$_3$), 120.8 (*para*-N-2,6-*i*Pr$_2$C$_6$H$_3$), 97.2 (C_8H_8), 29.1 (*C*HMe$_2$), 23.1 ppm (CH*Me*$_2$); IR (Nujol mull, NaCl plates): $\tilde{\nu}=1260$ (s), 1094 (br, s), 1018 (br, s), 800 (s), 670 cm^{-1} (w); EI-MS: *m/z*: 327 ([*M*]$^+$), 177 ([N-2,6-*i*Pr$_2$C$_6$H$_3$]$^+$), 162 ([2,6-*i*Pr$_2$C$_6$H$_3$]$^+$). HR EI-MS for [Ti(N-2,6-*i*Pr$_2$C$_6$H$_3$)(COT)]. Found (calcd for $C_{20}H_{25}NTi$): *m/z*: 327.1455 (327.1466); elemental analysis calcd (%) for $C_{20}H_{25}NTi$: C 73.4, H 7.7, N 4.3; found: C 70.4, H 7.6, N 4.2.

NMR-tube-scale synthesis of [Ti(N-2,6-*i*Pr$_2$C$_6$H$_3$)(COT′)] (4): To a solution of [Ti(N-2,6-*i*Pr$_2$C$_6$H$_3$)Cl$_2$(py)$_3$] (10 mg, 18 μmol) in C_6D_6 (0.3 mL) was added a solution of Li$_2$[COT′]·1.8THF (7.1 mg, 18 μmol) in C_6D_6 (0.1 mL). The reaction mixture was monitored by ^{1}H NMR for 16 h. During this time the quantitative conversion of [Ti(N-2,6-*i*Pr$_2$C$_6$H$_3$)Cl$_2$(py)$_3$] to [Ti(N-2,6-*i*Pr$_2$C$_6$H$_3$)(COT′)] (**4**) was observed.

^{1}H NMR data (C_6D_6, 300.0 MHz, 298 K): $\delta=7.28$ (s, 2H; 2- and 3-$C_8H_6(SiMe_3)_2$), 7.17 (m, 2H; 5- and 8-$C_8H_6(SiMe_3)_2$), 6.97 (m, 2H; 6- and 7-$C_8H_6(SiMe_3)_2$), 6.77 (d, $^3J=7.5$ Hz, 2H; *meta*-N-2,6-*i*Pr$_2$C$_6$H$_3$), 6.66 (t, $^3J=7.5$ Hz, 1H, *para*-N-2,6-*i*Pr$_2$C$_6$H$_3$), 3.32 (sept, $^3J=6.9$ Hz, 1H; C*H*Me$_2$), 1.16 (d, $^3J=6.9$ Hz, 12H; CH*Me*$_2$), 0.45 ppm (s, 18H; SiMe$_3$); ^{13}C{^{1}H} NMR data (C_6D_6, 75.5 MHz, 298 K): $\delta=159.1$ (*ipso*-N-2,6-*i*Pr$_2$C$_6$H$_3$), 139.1 (*ortho*-N-2,6-*i*Pr$_2$C$_6$H$_3$), 121.6 (*meta*-N-2,6-*i*Pr$_2$C$_6$H$_3$), 120.6 (*para*-N-2,6-*i*Pr$_2$C$_6$H$_3$), 108.1 (1- and 4-$C_8H_6(SiMe_3)_2$), 103.1 (2- and 3-$C_8H_6(SiMe_3)_2$), 101.5 (5- and 8-$C_8H_6(SiMe_3)_2$), 99.3 (6- and 7-$C_8H_6(SiMe_3)_2$), 28.7 (*C*HMe$_2$), 23.3 (CH*Me*$_2$), 0.7 ppm (SiMe$_3$).

[Ti(N-2-*t*BuC$_6$H$_4$)(COT′)] (5): To a stirred solution of [Ti(N-2-*t*BuC$_6$H$_4$)Cl$_2$(py)$_3$] (0.25 g, 0.50 mmol) in benzene (20 mL) was added a solution of Li$_2$[COT′]·1.8THF (0.20 g, 0.50 mmol) in benzene (10 mL) over 15 min. The reaction mixture was stirred for two days, during which time it became dark brown. The volatiles were removed under reduced pressure and the residue washed with pentane (3×15 mL). The solid was dried in vacuo to afford **5** as a light brown gum. Analysis by ^{1}H NMR spectroscopy indicated that the sample was sufficiently pure for further studies. Yield: 0.11 g (50%).

^{1}H NMR data (C_6D_6, 300.0 MHz, 298 K): $\delta=7.26$ (s, 2H; 2- and 3-$C_8H_6(SiMe_3)_2$), 7.17 (m, 2H, 5- and 8-$C_8H_6(SiMe_3)_2$), 6.98 (m, 2H, 6- and 7-$C_8H_6(SiMe_3)_2$), 6.93 (dd, $^2J_{65}=7.5$, $^3J_{64}=5.5$ Hz, 2H; 6-N-2-*t*BuC$_6$H$_4$), 6.71 (app dt, $J=7.2$ Hz, 1H; 5-N-2-*t*BuC$_6$H$_4$), 6.49 (app dt, $J=6.9$ Hz, 1H; 4-N-2-*t*BuC$_6$H$_4$), 6.18 (dd, $J=6.9$ Hz, 1H; 3-N-2-*t*BuC$_6$H$_4$), 1.43 (s, 9H; N-2-*tBu*C$_6$H$_4$), 0.45 ppm (s, 18H; SiMe$_3$); ^{13}C{^{1}H} data NMR (C_6D_6, 75.5 MHz, 298 K): $\delta=160.9$ (*ipso*-N-2-*t*BuC$_6$H$_4$), 137.5 (*ortho*-N-2-*t*BuC$_6$H$_4$), 132.4 (3-N-2-*t*BuC$_6$H$_4$), 125.7 (5- N-2-*t*BuC$_6$H$_4$), 125.0 (6- N-2-*t*BuC$_6$H$_4$), 119.6 (*para*- N-2-*t*BuC$_6$H$_4$), 107.4 (1- and 4-$C_8H_6(SiMe_3)_2$), 103.4 (2- and 3-$C_8H_6(SiMe_3)_2$), 101.5 (5- and 8-$C_8H_6(SiMe_3)_2$), 100.1 (6- and 7-$C_8H_6(SiMe_3)_2$), 34.8 (N*C*Me$_3$), 30.4 (NC*Me*$_3$), 0.5 ppm (SiMe$_3$); IR (Nujol mull, NaCl plates): $\tilde{\nu}=1260$ (s), 1091 (br, s), 1040 (s), 1019 (br, s), 837 (s), 831 (s), 751 (w), 721 cm^{-1} (w); EI-MS: *m/z*: 429 ([*M*−Me]$^+$), 281 ([Ti[COT′]−Me]$^+$), 133 ([2-*t*BuC$_6$H$_4$]$^+$), 73 ([SiMe$_3$]$^+$).

[Ti$_2$(μ-N-2,6-Me$_2$C$_6$H$_3$)$_2$(COT)$_2$] (6): To a stirred solution of [Ti(N-2,6-Me$_2$C$_6$H$_3$)Cl$_2$(py)$_3$] (0.44 g, 0.90 mmol) in benzene (20 mL) was added a solution of K$_2$[COT] (0.16 g, 0.90 mmol) in benzene (10 mL). The reaction mixture was stirred for two days, during which time it became dark brown and a solid precipitated out of solution. The solution was filtered and the black solid washed with pentane and dried in vacuo, to afford **6** as a black solid. Analysis by ^{1}H NMR spectroscopy indicated that the sample was sufficiently pure for further studies. A second crop of **6** was obtained by reducing the volume of the filtrate and cooling the remaining solution for one day at −30°C during which time a black solid precipitated out of solution. The solid was isolated by filtration, washed with pentane and dried in vacuo to afford a second crop of **6**. Yield: 0.12 g (49%). Black crystals suitable for X-ray diffraction were obtained from a saturated solution of [Ti$_2$(μ-N-2,6-Me$_2$C$_6$H$_3$)$_2$(COT)$_2$] in benzene at room temperature.

^{1}H NMR data (C_6D_6, 300.0 MHz, 298 K): $\delta=7.10$ (d, $^3J=7.2$ Hz, 4H; *meta*-N-2,6-Me$_2$C$_6$H$_3$), 6.85 (t, $^3J=7.2$ Hz, 2H; *para*-N-2,6-Me$_2$C$_6$H$_3$), 6.05 (s, 16H; C_8H_8), 2.10 ppm (s, 12H; N-2,6-*Me*$_2$C$_6$H$_3$); ^{13}C{^{1}H} NMR data (C_6D_6, 75.5 MHz, 298 K): $\delta=169.5$ (*ipso*-N-2,6-Me$_2$C$_6$H$_3$), 132.3 (*ortho*-N-2,6-Me$_2$C$_6$H$_3$), 121.5 (*para*-N-2,6-Me$_2$C$_6$H$_3$), 121.2 (*meta*-N-2,6-Me$_2$C$_6$H$_3$), 99.7 (C_8H_8), 20.3 ppm (N-2,6-*Me*$_2$C$_6$H$_3$); IR (Nujol mull, NaCl plates): $\tilde{\nu}=1260$ (m), 1214 (s), 1092 (br, m), 1020 (br, m), 802 (br, m), 770 (br, m), 722 cm^{-1} (s); UV data (benzene): $\lambda_{max}=$ 335 (2676), 386 (1901), 459 (850), 686 nm (236); EI-MS: *m/z*: 542 ([*M*]$^+$), 271 ([1/2*M*]$^+$), 167 ([1/2*M*−COT]$^+$), 152 ([1/2*M*−N-2,6-C$_6$H$_3$]$^+$); HR EI-MS for [Ti(N-2,6-Me$_2$C$_6$H$_3$)(COT)]$_2$: found (calcd for $C_{32}H_{34}N_2Ti_2$): *m/z*: 542.1667 (542.1681); elemental analysis calcd (%) or $C_{32}H_{34}N_2Ti_2$: C 70.9, H 6.3, N 5.2; found: C 69.5, H 6.0, N 5.1.

[Ti(N-2,6-Me$_2$C$_6$H$_3$)(COT′)] (7): To a stirred solution of [Ti(N-2,6-Me$_2$C$_6$H$_3$)Cl$_2$(py)$_3$] (0.25 g, 0.51 mmol) in benzene (20 mL) was added a solution of Li$_2$[COT′]·1.8THF (0.20 g, 0.51 mmol) in benzene (10 mL) over 15 min. The reaction mixture was stirred for two days, during which time it became dark brown. The volatiles were removed under reduced pressure and the residue washed with pentane (3×15 mL). The solid was dried in vacuo to afford **7** as an orange gum. Analysis by ^{1}H NMR spec-

troscopy indicated that the sample was sufficiently pure for further studies. Yield: 0.10 g (47 %).

^{1}H NMR data (C_6D_6, 300.0 MHz, 298 K): $\delta = 7.33$ (s, 2H; 2- and 3-$C_8H_6(SiMe_3)_2$), 7.20 (m, 2H; 5- and 8-$C_8H_6(SiMe_3)_2$), 6.93 (m, 2H; 6- and 7-$C_8H_6(SiMe_3)_2$), 6.74 (d, $^3J = 7.2$ Hz, 2H; *meta*-N-2,6-$Me_2C_6H_3$), 6.51 (t, $^3J = 7.2$ Hz, 1H; *para*-N-2,6-$Me_2C_6H_3$), 2.06 (s, 1H; N-2,6-$Me_2C_6H_3$), 0.45 ppm (s, 18H; $SiMe_3$); ^{13}C{^{1}H} NMR data (C_6D_6, 75.5 MHz, 298 K): $\delta = 161.5$ (*ipso*-N-2,6-$Me_2C_6H_3$), 128.9 (*ortho*-N-2,6-$Me_2C_6H_3$), 126.9 (*meta*-N-2,6-$Me_2C_6H_3$), 119.6 (*para*-N-2,6-$Me_2C_6H_3$), 107.2 (1- and 4-$C_8H_6(SiMe_3)_2$), 103.1 (2- and 3-$C_8H_6(SiMe_3)_2$), 101.2 (5- and 8-$C_8H_6(SiMe_3)_2$), 99.3 (6- and 7-$C_8H_6(SiMe_3)_2$), 33.1 (N-2,6-$Me_2C_6H_3$), 0.7 ppm ($SiMe_3$); IR (Nujol mull, NaCl plates): $\tilde{\nu} = 1260$ (s), 1090 (br, s), 1020 (br, s), 838 (s), 804 cm^{-1} (m); EI-MS: *m/z*: 415 ([*M*]$^+$), 248 ([COT″]$^+$), 106 ([N-2,6-C_6H_3]$^+$), 73 ([$SiMe_3$]$^+$); HR EI-MS for [Ti(N-2,6-$Me_2C_6H_3$)(COT″)]: found (calcd for $C_{22}H_{33}NSi_2Ti$): *m/z*: 415.1614 (415.1631); elemental analysis calcd (%) for $C_{22}H_{33}NSi_2Ti$: C 63.6, H 8.0, N 3.4; found: C 62.0, H 7.8, N 3.4.

The procedure described below for the synthesis of [$Ti_2(\mu$-$NPh)_2(COT'')_2$] (**8**), is also a representative procedure for *tert*-butylimido–aniline exchange reactions.

[$Ti_2(\mu$-$NPh)_2(COT'')_2$] (8): To a stirred solution of [Ti(N*t*Bu)(COT″)] (0.20 g, 0.54 mmol) in pentane (20 mL) was added a solution $PhNH_2$ (50 mg, 0.54 mmol) in pentane (10 mL). The reaction mixture was stirred for three days, during which time it became dark brown and a solid precipitated out of solution. The solid was isolated by filtration, washed with pentane (2×15 mL) and dried in vacuo to afford **8** as a light brown solid. Analysis by ^{1}H NMR spectroscopy indicated that the sample was sufficiently pure for further studies. Spectroscopically pure samples were obtained by recrystallisation at −30 C from a minimum amount of hexane. Yield: 0.14 g (68 %).

^{1}H NMR data (C_6D_6, 300.0 MHz, 298 K): $\delta = 7.25$ (t, $^2J = 7.5$ Hz, 4H; *ortho*-N-C_6H_5), 6.83 (t, $^2J = 7.5$ Hz, 2H; *para*-N-C_6H_5), 6.64 (m, 4H; 5- and 8-$C_8H_6(SiMe_3)_2$), 6.50 (s, 4H; 2- and 3-$C_8H_6(SiMe_3)_2$), 6.24 (app d, $J = 7.5$ Hz, 4H,; *meta*-N-C_6H_5), 6.03 (m, 2H; 6- and 7-$C_8H_6(SiMe_3)_2$), 0.43 ppm (s, 18H; $SiMe_3$); ^{13}C{^{1}H} NMR data (C_6D_6, 75.5 MHz, 298 K): $\delta = 169.1$ (*ipso*-N-C_6H_6), 128.0 (*ortho*-N-C_6H_6, obscured by solvent resonance), 120.3 (*para*-N-C_6H_6), 118.0 (*meta*-N-C_6H_6), 111.2 (1- and 4-$C_8H_6(SiMe_3)_2$), 106.4 (2- and 3-$C_8H_6(SiMe_3)_2$), 105.2 (5- and 8-$C_8H_6(SiMe_3)_2$), 102.1 (6- and 7-$C_8H_6(SiMe_3)_2$), 0.6 ppm ($SiMe_3$); IR (Nujol mull, NaCl plates): $\tilde{\nu} = 1260$ (s), 1244 (s), 1160 (br, s), 1092 (s), 1036 (s), 1020 (s), 840 (s), 804 (s), 746 cm^{-1} (m); EI-MS: *m/z*: 702 ([*M*−$SiMe_3$]$^+$), 387 ([1/2*M*]$^+$), 372 ([1/2*M*−Me]$^+$), 314 ([1/2*M*−$SiMe_3$]$^+$), 248 ([COT″]$^+$), 73 ([$SiMe_3$]$^+$); elemental analysis calcd (%) for $C_{40}H_{58}Si_4N_2Ti_2$: C 62.0, H 7.5, N 3.6; found: C 58.2, H 7.6, N 3.6.

Crystal structure determinations of [Ti(N*t*Bu)(COT)] (1), [Ti(N-2,6-*i*$Pr_2C_6H_3$)(COT)] (3), [$Ti_2(\mu$-N-2,6-$Me_2C_6H_3)_2(COT)_2$] (6): Crystal data collection and processing parameters are given in Table 7. Crystals were mounted on a glass fibre using perfluoropolyether oil and cooled rapidly to 150 K in a stream of cold N_2 using an Oxford Cryosystems CRYOSTREAM unit. Diffraction data were measured by using either a Stoë Stadi-4 four-circle diffractometer (for **1**) or an Enraf-Nonius KappaCCD diffractometer (for **3** and **6**). Intensity data for **1** were processed using X-RED,[61] and those for **3** and **6** were processed using the DENZO-SMN package.[62] The structures were solved by using the direct methods program SIR92,[63] which located all non-hydrogen atoms. Subsequent full-matrix least-squares refinement was carried out using the CRYSTALS program suite.[64] Coordinates and anisotropic thermal parameters of all non-hydrogen atoms were refined. Hydrogen atoms were positioned geometrically. Weighting schemes were applied as appropriate.

Data for **1** were collected to a θ_{max} of only 22.5° due to the weakly diffracting nature of the crystal, to which we also attribute the high conventional R_1 value of 0.094. Numerical absorption corrections by means of face indexing were not applicable due to the irregular shape of the crystal and its encapsulation in a film of perfluoropolyether. The residual electron density peaks peaks of +3.2 to −1.6 eÅ^{-3} found after refinement on data corrected for absorption using Ψ scans were considerably reduced on the application of DIFABS.[65] The value of 0.71 for E^2–1 (E = normalised structure factor) suggested possible twinning but no useable twin law could be found. Repeated attempts to grow better diffraction-quality crystals were unsuccessful.

Table 7. Crystal data collection and processing parameters for [Ti(N*t*-Bu)(COT)] (**1**), [Ti(N-2,6-*i*$Pr_2C_6H_3$)(COT)] (**3**) and [$Ti_2(\mu$-N-2,6-$Me_2C_6H_3)_2(COT)_2$] (**6**).

	1	**3**	**6**
empirical formula	$C_{12}H_{17}NTi$	$C_{20}H_{25}NTi$	$C_{32}H_{34}N_2Ti_2$
Fw	223.17	327.33	542.44
T [K]	150	150	150
wavelength [Å]	0.710713	0.710713	0.710713
space group	$P\bar{1}$	$C2/c$	$Pbcn$
a [Å]	6.255(3)	11.0871(3)	9.6785(3)
b [Å]	8.980(4)	18.0712(6)	13.6629(4)
c [Å]	11.144(6)	10.1847(3)	19.2015(6)
α [°]	82.58(6)	90	90
β [°]	89.74(4)	119.7502(12)	90
γ [°]	70.51(6)	90	90
V [Å^3]	584.7(8)	1771.62(9)	2539.14(13)
Z	2	4	8
ρ_{calcd} [Mg m^{-3}]	1.270	1.227	1.419
μ [mm^{-1}]	0.690	0.480	0.654
R indices R_1, R_w [$I > 3\sigma(I)$]	$R_1 = 0.094$ $R_w = 0.097$	$R_1 = 0.032$ $R_w = 0.037$	$R_1 = 0.040$ $R_w = 0.046$

CCDC-117841, CCDC-262147 and CCDC-262148 contain the supplementary crystallographic data for this paper. These data can be obtained free of charge from The Cambridge Crystallographic Data Centre via www.ccdc.cam.ac.uk/data_request/cif.

Acknowledgements

This work was supported by funding from the EPSRC and Rhodes Trust. We thank Professors F. G. N. Cloke and J. D. Protasiewicz for valuable advice and discussions and CCLRC Daresbury Laboratory for access to CSD. Calculations were carried out by using the facilities of the Oxford Supercomputing Centre.

[1] D. E. Wigley, *Prog. Inorg. Chem.* **1994**, *42*, 239–482.
[2] T. R. Cundari, *J. Am. Chem. Soc.* **1992**, *114*, 7879–7888.
[3] T. R. Cundari, *Chem. Rev.* **2000**, *100*, 807–818.
[4] A. P. Duncan, R. G. Bergman, *Chem. Rec.* **2002**, *2*, 431–445.
[5] L. H. Gade, P. Mountford, *Coord. Chem. Rev.* **2001**, *216–217*, 65–97.
[6] P. Mountford, *Chem. Commun.* **1997**, 2127–2134.
[7] U. Radius, *Z. Anorg. Allg. Chem.* **2004**, *630*, 957–972.
[8] C. C. Cummins, S. M. Baxter, P. T. Wolczanski, *J. Am. Chem. Soc.* **1988**, *110*, 8731–8733.
[9] C. C. Cummins, C. P. Schaller, G. D. Van Duyne, P. T. Wolczanski, A. W. E. Chan, R. Hofmann, *J. Am. Chem. Soc.* **1991**, *113*, 2985–2994.
[10] J. L. Bennett, P. T. Wolczanski, *J. Am. Chem. Soc.* **1994**, *116*, 2179–2180.
[11] C. P. Schaller, C. C. Cummins, P. T. Wolczanski, *J. Am. Chem. Soc.* **1996**, *118*, 591–611.
[12] J. L. Bennett, P. T. Wolczanski, *J. Am. Chem. Soc.* **1997**, *119*, 10696–10719.
[13] P. J. Walsh, F. J. Hollander, R. G. Bergman, *J. Am. Chem. Soc.* **1988**, *110*, 8729.
[14] P. J. Walsh, F. J. Hollander, R. G. Bergman, *Organometallics* **1993**, *12*, 3705–3723.
[15] H. M. Hoyt, M. E. Forrest, R. G. Bergman, *J. Am. Chem. Soc.* **2004**, *126*, 1018–1019.
[16] A. J. Blake, P. E. Collier, L. H. Gade, M. McPartlin, P. Mountford, M. Schröder, *Chem. Commun.* **1997**, 1555–1556.

[17] C. H. Winter, P. H. Sheridan, T. S. Lewkebandara, M. J. Heeg, J. W. Proscia, *J. Am. Chem. Soc.* **1992**, *114*, 1095–1097.
[18] C. J. Carmalt, S. R. Whaley, P. S. Lall, A. H. Cowley, R. A. Jones, B. G. McBurnett, J. G. Ekerdt, *J. Chem. Soc. Dalton Trans.* **1998**, 553–557.
[19] C. J. Carmalt, A. C. Newport, I. P. Parkin, A. J. P. White, D. J. Williams, *Chem. Commun.* **2002**, 4055–4059.
[20] C. J. Carmalt, A. C. Newport, I. P. Parkin, P. Mountford, A. J. Sealey, S. R. Dubberley, *J. Mater. Chem.* **2003**, *13*, 84–87.
[21] A. J. Nielson, M. W. Glenny, C. E. F. Rickard, *J. Chem. Soc. Dalton Trans.* **2001**, 232–239.
[22] N. A. H. Male, M. E. G. Skinner, S. Y. Bylikin, P. J. Wilson, P. Mountford, M. Schröder, *Inorg. Chem.* **2000**, *39*, 5483–5491.
[23] N. Adams, H. J. Arts, P. D. Bolton, D. Cowell, S. R. Dubberley, N. Friederichs, C. Grant, M. Kranenbrug, A. J. Sealey, B. Wang, P. J. Wilson, A. R. Cowley, P. Mountford, M. Schröder, *Chem. Commun.* **2004**, 434–435.
[24] J. E. Hill, R. D. Profilet, P. E. Fanwick, I. P. Rothwell, *Angew. Chem.* ***1990****, 102, 713–715; Angew. Chem. Int. Ed. Engl.* **1990**, *29*, 664–665.
[25] P. H. Roesky, H. Voelker, M. Witt, M. Noltemeyer, *Angew. Chem.* ***1990****, 102, 73–74; Angew. Chem. Int. Ed. Engl.* **1990**, *29*, 669–670.
[26] A. J. Blake, P. E. Collier, S. C. Dunn, W. Li, P. Mountford, O. V. Shishkin, *J. Chem. Soc. Dalton Trans.* **1997**, 1549–1558.
[27] D. J. Arney, M. A. Bruck, S. R. Huber, D. E. Wigley, *Inorg. Chem.* **1992**, *31*, 3749–3755.
[28] D. S. Glueck, J. Wu, F. J. Hollander, R. G. Bergman, *J. Am. Chem. Soc.* **1991**, *113*, 2041–2054.
[29] R. I. Michelman, R. A. Anderson, R. G. Bergman, *J. Am. Chem. Soc.* **1991**, *113*, 5100–5102.
[30] A. J. Blake, S. C. Dunn, J. C. Green, N. M. Jones, A. G. Moody, P. Mountford, *Chem. Commun.* **1998**, 1235–1236.
[31] F. G. N. Cloke in *Comprehensive Organometallic Chemistry Vol. 4* (Eds: E. W. Abel, F. G. A. Stone, G. Wilkinson), Elsevier, New York, **1995**.
[32] D. A. Fletcher, R. F. McMeeking, D. Parkin, *J. Chem. Inf. Comput. Sci.* **1996**, *36*, 746–749.
[33] F. H. Allen, O. Kennard, *Chem. Des. Autom. News* **1993**, *8*, 31.
[34] W. A. Nugent, B. L. Haymore, *Coord. Chem. Rev.* **1980**, *31*, 123–175.
[35] D. L. Thorn, W. A. Nugent, R. L. Harlow, *J. Am. Chem. Soc.* **1981**, *103*, 357–363.
[36] S. Gambarotta, C. Floriani, A. Chiesi-Villa, C. Guastini, *J. Am. Chem. Soc.* **1983**, *105*, 7295–7301.
[37] W. J. Grigsby, M. M. Olmstead, P. P. Power, *J. Organomet. Chem.* **1996**, *513*, 173–180.
[38] J. C. Gordon, G. R. Giesbrecht, D. R. Clark, P. J. Hay, D. W. Keogh, R. Poli, B. L. Scott, J. G. Watkin, *Organometallics* **2002**, *21*, 4726–4734.
[39] J. G. Brennan, R. A. Andersen, A. Zalkin, *J. Am. Chem. Soc.* **1988**, *110*, 4554–4558.
[40] J. L. Stewart, R. A. Andersen, *New J. Chem.* **1995**, *19*, 587.
[41] R. C. Schnabel, B. L. Scott, W. H. Smith, C. J. Burns, *J. Organomet. Chem.* **1999**, *591*, 14–23.
[42] P. L. Diaconescu, P. L. Arnold, T. A. Baker, D. J. Mindiola, C. C. Cummins, *J. Am. Chem. Soc.* **2000**, *122*, 6108–6109.
[43] M. Elian, M. M. L. Chen, M. P. Mingos, R. Hoffmann, *Inorg. Chem.* **1976**, *15*, 1148–1155.
[44] R. R. Andréa, A. Terpstra, A. Oskam, P. Bruin, J. H. Teuben, *J. Organomet. Chem.* **1986**, *307*, 307–317.
[45] D. S. Glueck, J. C. Green, R. I. Michelman, I. N. Wright, *Organometallics* **1992**, *11*, 4221–4225.
[46] R. B. King, *Organometallic Synthesis*, Academic Press, New York and London, **1965**.
[47] C. N. Field, J. C. Green, M. Mayer, V. A. Nasluzov, N. Rosch, M. R. F. Siggel, *Inorg. Chem.* **1996**, *35*, 2504–2514.
[48] X. Li, J. S. Tse, G. M. Bancroft, R. J. Puddephatt, K. H. Tan, *Inorg. Chem.* **1996**, *35*, 2515–2523.
[49] E. J. Baerends, J. A. Autschbach, A. Berces, C. Bo, P. M. Boeringter, L. Cavallo, D. P. Chong, L. Deng, R. M. Dickson, D. E. Ellis, L. Fan, T. H. Fischer, C. Fonesca Guerra, S. J. A. Van Gisbergen, J. A. Groeneveld, O. V. Gritsenko, M. Grüning, F. E. Harris, P. van den Hoek, H. Jacobsen, G. van Kessel, F. Kootstra, E. Vanlenthe, V. P. Osinga, S. Patchkovskii, P. H. T. Phillipsen, D. Post, C. C. Pye, W. Ravenek, P. Ros, P. R. T. Schipper, G. Schreckenbach, J. G. Snijders, M. Sola, M. Swart, D. Swerhone, G. te Velde, P. Vernooijis, L. Versluis, O. Visser, E. van Wezenbeek, G. Wiesenekker, S. K. Wolff, T. K. Woo, T. Ziegler, *Scientific Computing and Modelling NV Vrije Universiteit, Amsterdam* **2002**.
[50] E. Vanlenthe, E. J. Baerends, J. G. Snijders, *J. Chem. Phys.* **1993**, *99*, 4597–4610.
[51] E. Vanlenthe, E. J. Baerends, J. G. Snijders, *J. Chem. Phys.* **1994**, *101*, 9783–9792.
[52] E. Vanlenthe, E. J. Baerends, J. G. Snijders, *J. Chem. Phys.* **1996**, *105*, 6505–6516.
[53] E. Vanlenthe, R. VanLeeuwen, E. J. Baerends, J. G. Snijders, *Int. J. Quantum Chem.* **1996**, *57*, 281–293.
[54] E. Vanlenthe, A. Ehlers, E. J. Baerends, *J. Chem. Phys.* **1999**, *110*, 8943–8953.
[55] S. H. Vosko, L. Wilk, M. Nusair, *Can. J. Phys.* **1980**, *58*, 1200–1211.
[56] A. D. Becke, *Phys. Rev. A* **1988**, *38*, 3098–3100.
[57] A. D. Becke, *J. Chem. Phys.* **1988**, *88*, 1053–1062.
[58] J. P. Perdew, *Phys. Rev. B* **1986**, *33*, 8800.
[59] T. M. Gilbert, R. R. Ryan, A. P. Sattelberger, *Organometallics* **1988**, *7*, 2514–2518.
[60] N. C. Burton, F. G. N. Cloke, S. C. P. Joseph, H. Karamallakis, A. A. Sameh, *J. Organomet. Chem.* **1993**, *462*, 39–43.
[61] S. Corporation, *X-RED data reduction program, version 1.09 for windows,* **1997**.
[62] Z. Otwinowski and W. Minor, *Processing of X-ray Diffraction Data Collected in Oscillation Mode, Methods Enzymology*, Academic Press, **1997**.
[63] A. Altomare, G. Cascarano, G. Giacovazzo, A. Guagliardi, M. C. Burla, G. Polidori, M. Camalli, *J. Appl. Crystallogr.***1994**, *27*, 435.
[64] P. W. Betteridge, J. R. Cooper, R. I. Cooper, K. Prout, D. J. Watkin, *J. Appl. Crystallogr.* **2003**, *36*, 1487.
[65] N. Walker, D. Stuart, *Acta Crystallogr. Sect. A* **1983**, *39*, 158.
[66] We have recently shown that the reaction of [Ti(N*t*Bu)(COT)] (**1**) with pyridine forms the 18 electron complex [Ti(N*t*Bu)(COT)(py)]. The molecular structure of [Ti(N*t*Bu)(COT)(py)] has been obtained and the ring-Ti–N bond angle is clearly bent. A manuscript containing this work is currently in preparation.

Received: November 2, 2004
Published online: February 15, 2005